EUROPEAN COMMISSION

nuclear science and technology

Assessment of Aged Piping Dissimilar Metal Weld Integrity (ADIMEW)

Contract FIKS-CT2000-00047

Final report

Work performed as part of the European Atomic Energy Community's research and training programme in the field of nuclear energy 1998-2002 (Fifth Framework Programme)
Key action: Nuclear fission
Area: Operational safety of existing installations

Directorate-General for Research
2008 Euratom EUR 23315

Project coordinator

C. Faidy, EDF-SEPTEN, France

Project partners

G. Martin, EDF-DRD-MTC, France

N. Taylor, A. Youtsos, and D. Katsareas, JRC-IE, EC

H. Keinanen and A. Laukkanen, VTT, Finland

J. Wintle, TWI, UK

A. Sherry and D. Lidbury, Serco Assurance, UK

N. Safa, M. F. Cipiere, and P. Gilles, Framatome-ANP, France

S. Chapuliot and Y. Kaiser, CEA, France

G. Lenkey, BZF, Hungary

Contents

General presentation

The objective of the three-year ADIMEW project, which started in November 2000, was to contribute to the development and verification of analysis methods that describe the behaviour of cracked dissimilar metal welds (DMW). The complexity of the problem results from the prevailing mixed-mode loading conditions, the variation in material constitutive equations across the weld zone, and the presence of large residual stress fields. Under these circumstances, classic fracture mechanics concepts are difficult to apply.

The project had the following technological and scientific aims:

- Quantify the accuracy and conservatism of structural integrity procedures used by the nuclear industry in Europe to predict the behaviour and assess the safety of circumferential defects at the surface of dissimilar metal welds
- Perform a unique verification of the load-carrying capacity of an industrially representative cracked DMW under operating conditions in a large-scale structural test. To do this, a special assembly was prepared, with circumferential cracks introduced into the surface of a dissimilar metal weld between low-alloy steel and austenitic steel pipes with a diameter of 450 mm
- Rapidly disseminate the results for the benefit of operators, regulators and research organisations in Europe, in collaboration with the Network for Evaluating Structural Components (NESC).

In order to reach these objectives, a large-scale nuclear DMW was tested and the different analytical methods available checked against the experimental results. Complementary innovative actions have been done on mixed-mode rupture, comparison of notch and crack toughness values.

The ADIMEW project had an organisation similar to the one of the BIMET project [1] with complementary objectives: larger diameter and higher temperature.

The ADIMEW project followed on from the successful Fourth Framework Programme (FP4) BIMET project [1] which had complementary objectives but considered smaller-diameter weld mock-ups tested at ambient rather than service temperature.

The main focus of ADIMEW project was the performance of a single benchmark 4-point bend-pipe test, conducted on a nominal 16" piping assembly at 300 °C and containing a ferritic to stainless-steel (A508-308/309SS-316SS) DMW. A notch-like defect was inserted at the ferritic steel/buttering layer interface, to simulate plant experience of damage at the worst-case location for a crack in such components. A second DMW mock-up was also manufactured for the experimental determination of welding residual stresses and for the generation of material property data for input to the analysis procedures. A range of analysis methodologies, including conventional flaw assessment methods, J approaches and local-approach methods have been applied to predict the critical load for initiation of the defect, the extent of crack growth, and the path followed by the crack through the weld up to the maximum load. Consideration has also been given to factors such as welding residual stresses, mixed-mode loading and constraint effects.

The ADIMEW test was successfully executed in July 2003. The complete results of investigations of the test pieces were available in October 2003 and the post-test analysis was completed by December 2003.

1. Project description

1.1. Mock-up fabrication and defect insertion

The ADIMEW project plan required the procurement of materials and fabrication of two dissimilar weld mock-ups (denominated AD01 and AD02) fully representative of the 16" diameter girth weld connecting the pressuriser to the surge line of a French N4 plant. To guarantee the quality of the DMWs, a considerable experience and high degree of quality control has been required within the weld manufacturing process, in accordance with Framatome basic nuclear specifications [2] for French nuclear power plants. The parent pipe materials are on one side a forged low alloy steel (SA508 Cl3) and on the other part a forged stainless steel (316L). The two-layer buttering is done with 308 L and 309 L filler metal and the weld with 308 L filler metal (more than 90 weld passes). The overall DMW dimensions were 1040 mm length, 51 mm wall thickness and 453 mm outer diameter (Fig. 1).

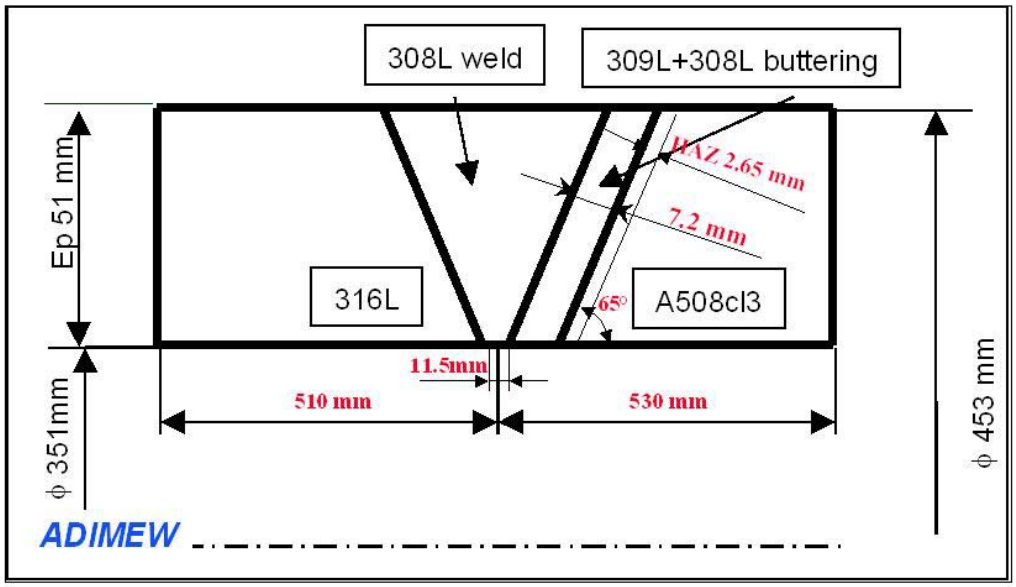

Figure 1: AD02 – Mock-up geometry

Figure 2 summarises the materials used and the specifications for the fabrication process. It can be seen that different NDE examinations (ultrasonic, radiographic and die penetrant tests) were performed at the end of the buttering and the weld fabrication stages. At the end of the welding a final post weld heat treatment was done (6 hours between 595 and 600 °C). Full details of the process are presented in [2]. Two identical mock-ups were produced: AD01 for the residual stress measurements and the materials properties investigations and AD02 for the actual ADIMEW bend test.

It is also noted that during the production of the second AD02 mock-up, the temperature and heat input history was recorded for latter use in the finite element modelling activities associated with the prediction of the weld residual stress fields. This included detailed strain gauge and

thermocouples information have been recorded continuously during the welding [1]. Figure 3 shows a cross-section of the weld, taken from the AD01 mock-up during the material characterisation studies.

Base materials
A 508 cl.3 type forged ferritic steel, length: 500 mm
316L (Z2 CND 18-12) austenitic stainless steel, length: 500 mm

Weld metal
Covered electrode 24/12 (309L) and 20/12 (308L) for the buttering
Covered electrode 20/10 (308L) for the weld

Fabrication
(1) Buttering:
- Preheating : $\theta > 150$ °C
- Interpass temperature: $\theta < 250$°C
- First layer: 309L – diameter: $\Phi = 4$ mm, current: 90 to 160 A
- Further layers: 308L,
(1) diameter: $\Phi = 4$ mm, current: 115 to 145 A,
(2) diameter: $\Phi = 5$ mm, current : 170 to 200 A
- Post-heating: 250 °C < θ < 400 °C , holding time > 4 hours
- Machining
- Non-destructive tests

(2) Weld:
- Welding: 308L
- Diameter: $\Phi = 4$ mm, current: 115 to 145 A
- Diameter: $\Phi = 5$ mm, current: 170 to 200 A
- Interpass temperature: $\theta < 250$°C
- Stress relief heat treatment: 595-620 °C, holding time: 2h15-2h45
- Final machining
- Non-destructive tests

Figure 2: Mock-up material and fabrication specifications

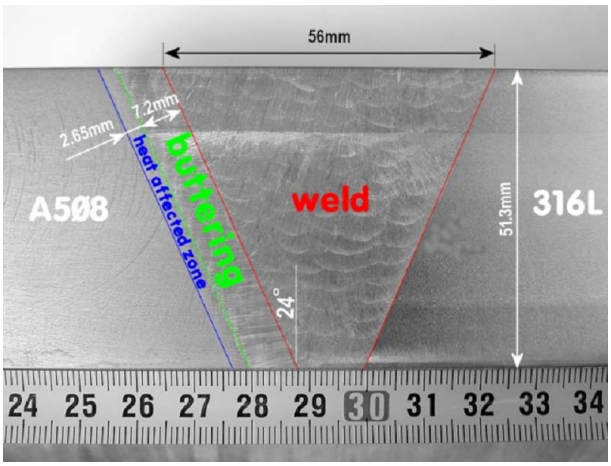

Figure 3: Cross-section of the bimetallic weld of AD01

The next step in the preparation of the test mock-up involved the insertion of a simulated crack-like defect in the AD02 weld. An initial design analysis was undertaken to establish the size of defect required to guarantee propagation during the test and within the loading capacity of the proposed EDF testing facility. The final specification called for a partial circumferential defect with a maximum depth of third of the wall thickness (Fig. 4).

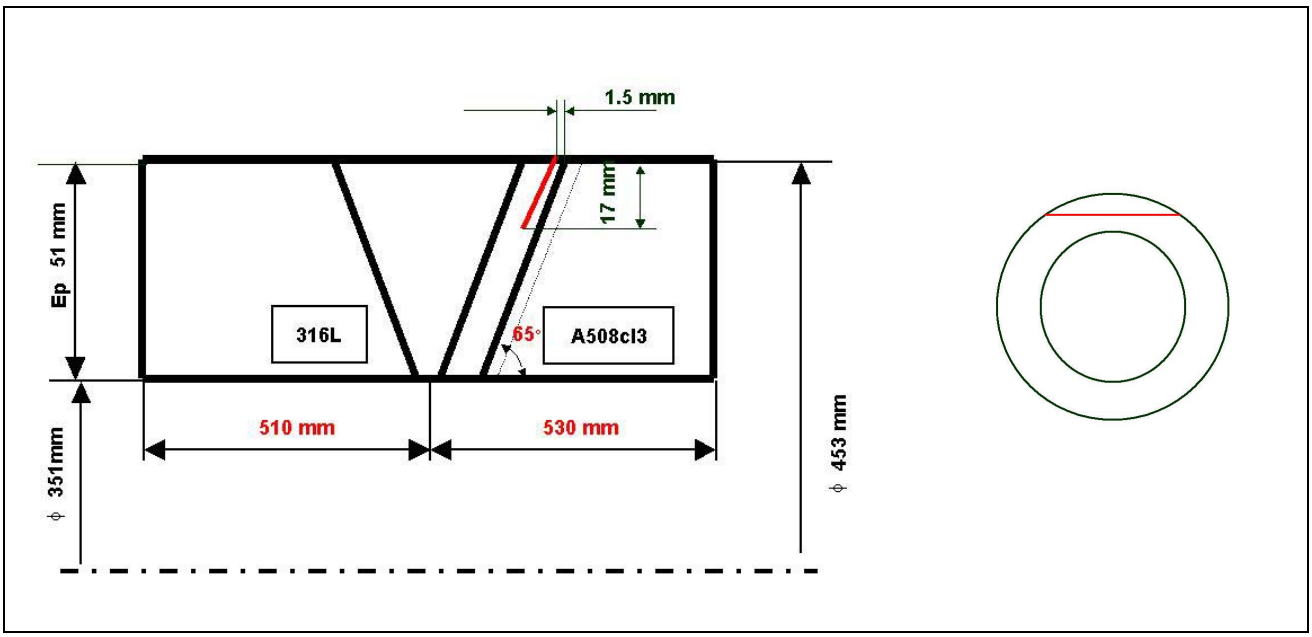

Figure 4: AD02 – Crack size, location and shape

The defect was produced by means of electro-discharge machining (Fig. 5). A complete trial was performed on a specially prepared dummy weld to insert a 25 mm defect with the same procedure and same electrode. This allowed optimisation of the EDM machining procedure and to define the maximum feasible depth of the defect [3]. The precise location of the defect within the weld was a critical issue and great care has been applied during the defect insertion procedure (Fig. 6-7).

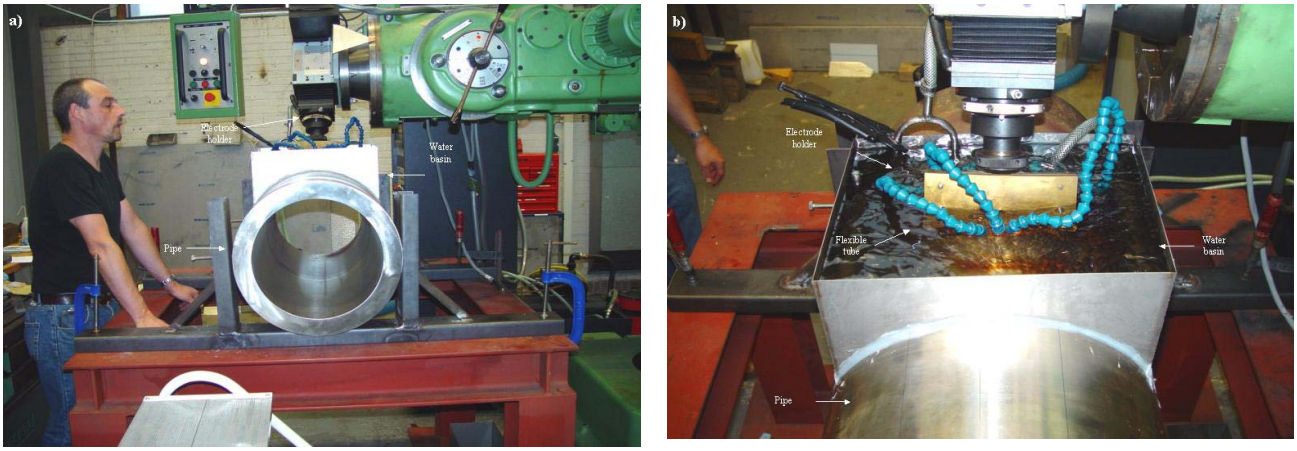

Figure 5: Defect insertion equipment : (a) overview (b) detailed view

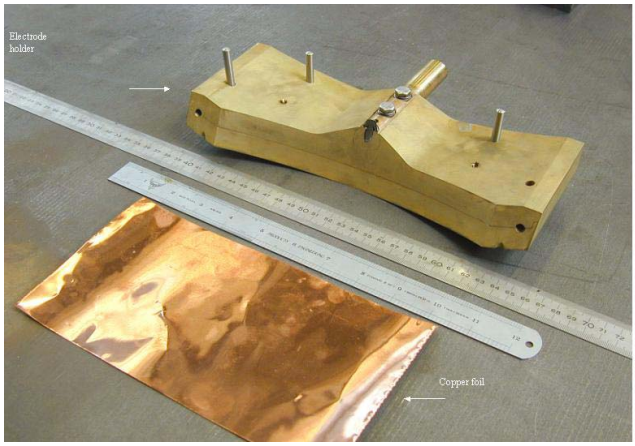

Figure 6: Electrode holder and copper foil for defect insertion

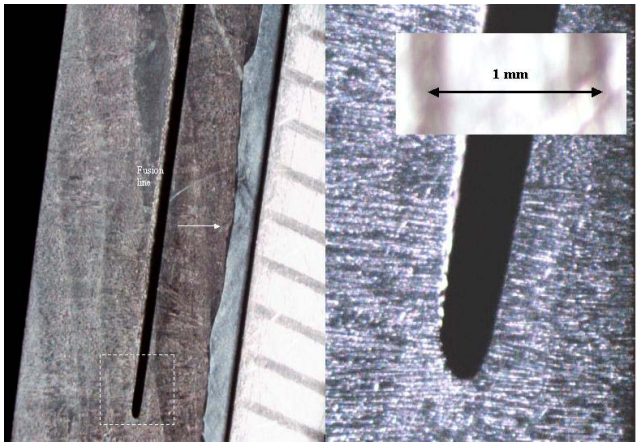

Figure 7: Shape of the 25 mm deep defect inserted into the trial DMW

Finally the crack has been machined in the buttering 1.5mm from the fusion line; the corresponding crack tip radius is around 0.4 mm. After the machining of the defect, the defect shape was controlled by means of taking replicas. The defect depth variation is less than $\pm$ 0.15 mm.

As the final step in the fabrication of the test assembly, extension arms were welded to the DMW section part in order to form a 7m assembly of around 7 tones weight (Fig. 8). These arms are in a high strength carbon steel to assure them an elastic behaviour all along the test [4].

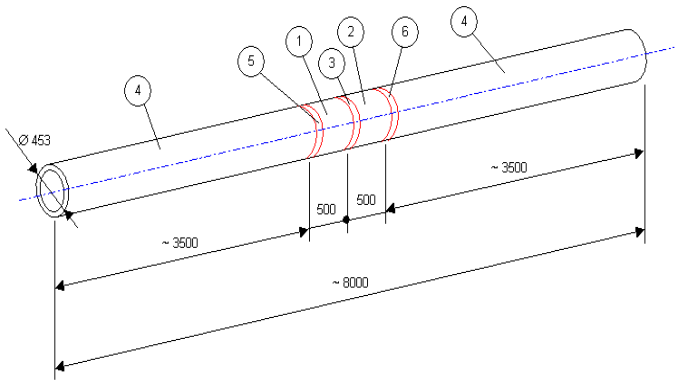

Figure 8: The component geometry and materials:
1 - Austenitic base metal, 2 - Ferritic base metal, 3 - Dissimilar metal weld, 4 - Prolongation arms, 5 - Weld connecting austenitic base metal to prolongation arm, 6 - Weld connecting ferritic base metal to prolongation arm

1.2. Material characterisation

The analysis work requires extensive materials characterisation around the fusion line: strength, ductility and fracture behaviour of the weld heat affected zones and the dissimilar parent metals. J_{IC}-values and fracture resistance (R) curves, characterising the fracture initiation toughness and ductile crack growth, respectively, are required as inputs to the structural integrity analyses.

The materials characterisation task has required a considerable degree of innovation and the application of the most recent pre-normative testing technologies.

The base materials comprise a ferritic low-alloy steel SA508 and an austenitic stainless steel AISI 316 L. As filler metals, over-alloyed Ni-enriched E 309 L (24 % Cr, 12 % Ni) was used for the first buttering layer, whilst matching E 308L (18 % Cr, 8 % Ni) was used to deposit the buttering layers and to complete the final weld.

The performed material characterisation program is presented in Table 1. Hardness, stress-strain curves and fracture resistance are measured for different material at two different temperatures (20 and 300 °C), using international standardised procedures.

The component geometry and materials are presented in Fig. 3 and 8.

Organisation	**Specimen type**	**Specimen dimensions** (mm)	**Specimen location**	**Number of tests and temperature**		**Type of test and standard**
		B, W, L		25 °C	300 °C	
Framatome ANP	CVN	10,10,55	BU_{FL}	8	8	transition curve
	CVN	10,10,55	BM1, BM2 WM	8	8	to define upper shelf
	CT 25 SG	25,50	BU_{FL}	≥3**	≥5**	J_{IC}, K_{JC}, JR (full size R-curve)
TWI	SENB normal	20,40,100	BU_{FL}		3**	J_R unloading compliance
	SENB sub size	10,10,55	BU_{FL} FL_{BU} CGHAZ WM		3 2 1 3	J_R unloading compliance
VTT	SENB sub size	10,10,55	BU_{FL} FL_{CGHAZ} WM	2* 2* 2		J_{IC}, K_{JC}, JR (sub size R-curve) ASTM E1737-96
	SENB sub size	10,10,55	BU_{FL} FL_{CGHAZ}	4* 4*		mixed mode R-curve
	Tensile/ round bar	Φ = 2...5 mm	BU_{FL} BU WM BM1 BM2	2 2 2 2 2	2 2 2 2 2	stress-strain/strength, deformation parameters
	Tensile/flat miniature	cross section of $1\times 2\ mm^2$	BU_{FL} FL_{CGHAZ} WM	2 2 2	2 2 2	local tensile properties
BZF	CT25	25,50,60	BU_{FL}	1	4	R-curve, effect of notch tip radius ASTM E 1820-99a

- BU_{FL} indicates the notch is located in the weld buttering 1-2 mm from the fusion line
- FL_{BU} indicates the notch is located on the fusion line tending towards the buttering side
- CGHAZ indicate the notch is located in the coarse grained heat affected zone
- WM indicates that the notch is located in the bulk weld metal, with the notch direction parallel to the fusion line in all cases
- BM = base material (BM1 = ferritic, BM2 = austenitic)

Table 1: Test matrix for ADIMEW

A specific attention was on the comparison of toughness measured on a pre-fatigue cracked specimen versus a notch specimen similar to the ADIMEW cracked mock-up. The mock-up with the "window" cuts for the residual stress measurements and material characterisation is shown in Fig. 9 and 10. The slices were cut from the both ends of the mock-up.

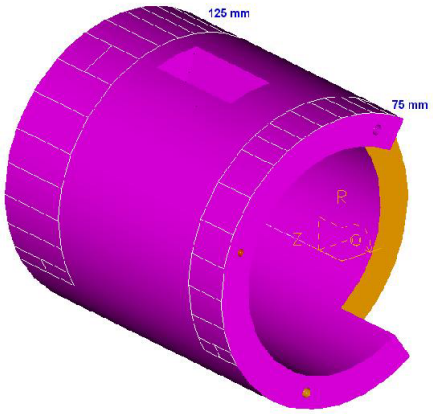

Figure 9: Mock-up with windows for neutron diffraction measurements

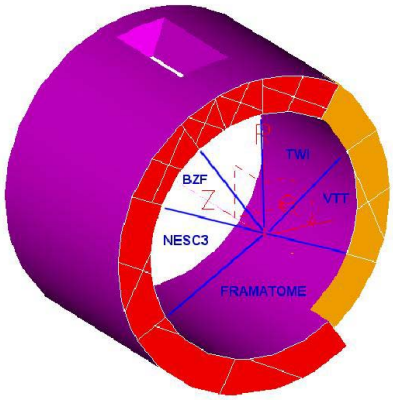

Figure 10: Blocks used by each partners

Hardness measurements

Regarding the hardness test results, Fig. 11, it should first of all be remarked that no significant trends could be discovered within either base metal (A508 & 316L), weld (308L) or buttering layer (308L & 309L). Some remarkable low values were indicated in italics. Further you will notice that the weld metal, i.e. both the butt weld and the buttering, is quite hard, as compared with the ferritic base metal. Especially the second buttering layer (308L) shows high hardness figures. If the averages from all the measurements are considered, the following values are obtained:

- austenitic base metal 316L: 152
- butt weld metal E308L: 202
- second buttering layer E308L: 215
- first buttering layer E309L: 200
- ferritic base metal A508: Cl3.

So there is no gradual transition from the austenitic to the ferritic base metal.

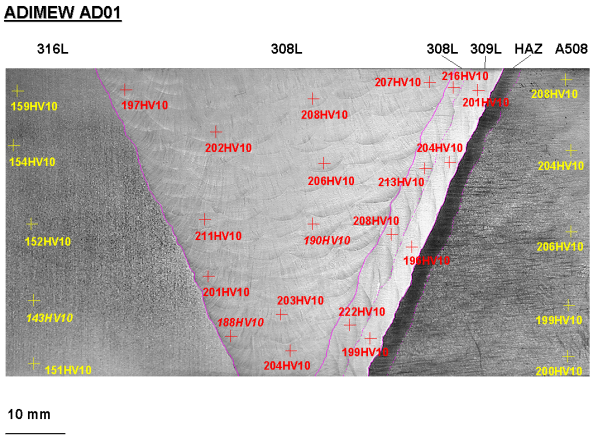

Figure 11: Hardness measurement results

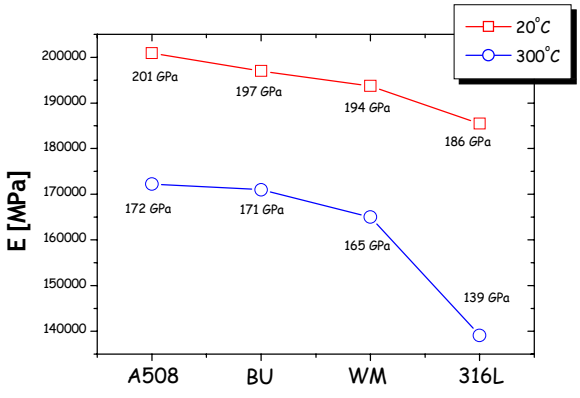

Figure 12: Elastic modulus values

Engineering stress-strain curves

The major results are presented in table 2 for different locations and different temperature (20 and 300 °C). Specific attention was given to Young's modulus evaluation and the results are presented Fig. 12.

REGION	Temperature [°C]	σ_{ys} [MPa]†	σ_{ts} [MPa]‡	E [GPa]
316L	20	294	592	186
316L	300	213	453	139
A508	20	513	671	201
A508	300	463	640	172
WM	20	370	636	194
WM	300	346	441	165
BU	20	418	615	197
BU	300	349	462	171

† engineering definition of yield strength
‡ tensile strength

Table 2: Engineering stress-strain curves results

Fracture toughness and J-R curves

The fracture resistance curves of the sub-size SENB test program [5] at ambient temperature are presented in Fig. 13, 14 and 15. The initiation fracture toughness results are collected in Fig. 16 and Table 3. The FL region results are seen to depict considerable scatter and dependency on sectioning thickness, whilst the JR curve slope after crack initiation is nearly negligible. The fracture toughness of the ferritic HAZ is seen to exceed the FL region, considering, both for cracks placed near and at the FL. The fracture resistance of the BU increases remarkably further away from the FL.

Specimen location	E1820, J_{1c} (kJ/m^2)
FL t/3	267
FL t/3	156
$BU_{FL\ (0.5mm)}$ 2t/3	249
$BU_{FL\ (0.5mm)}$ t/3	173
$HAZ_{\ (0.5mm)}$ 2t/3	499
$HAZ_{\ (0.5mm)}$ t/3	501
$BU_{(2mm)}$ 2t/3	308
$BU_{(2mm)}$ 2t/3	272

Table 3: Initiation fracture toughness values

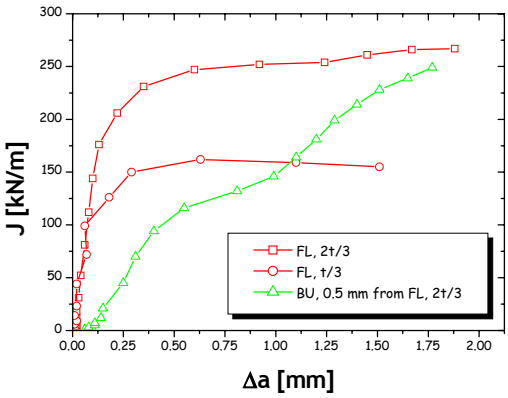

Figure 13: Fracture resistance curves of CVN size SENBs at ambient temperature for the FL and BU regions. The BU curve crack is nominally located 0.5 mm from FL

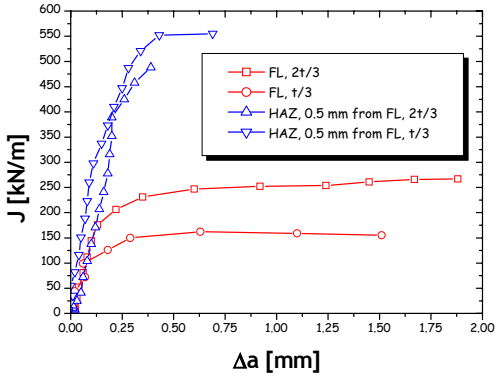

Figure 14: Fracture resistance curves of CVN size SENBs at ambient temperature for the FL and ferritic HAZ regions. The HAZ curve crack is nominally located 0.5 mm from FL

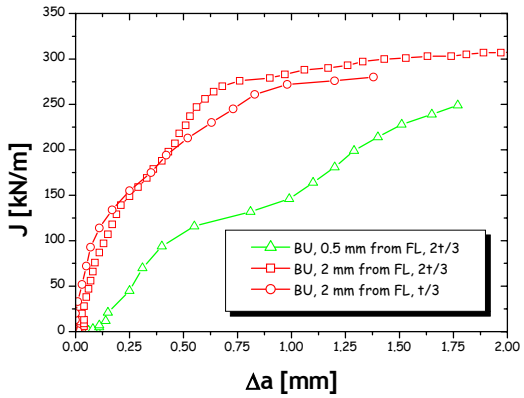

Figure 15: Fracture resistance curves of CVN size SENBs at ambient temperature for the BU region, nominal locations 0.5 mm and 2 mm from the FL, respectively

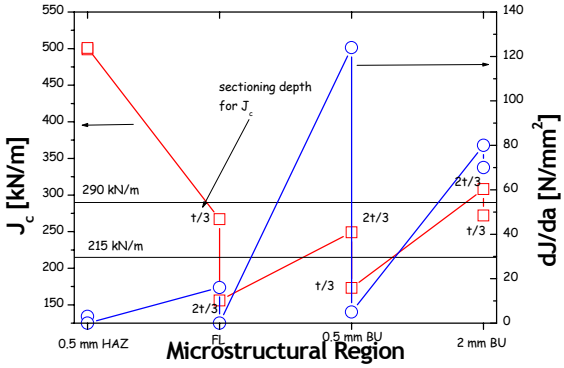

Figure 16: Collected initiation fracture toughness and JR curve slope results for CVN-size SENBs at ambient temperature. Sectioning thickness illustrated as t/3 and 2t/3, respectively

Complementary toughness values of the buttering from impact test and CTJE25 specimen

Impact notch tests with specimen of Charpy V-notch type were performed for all base metals, low alloy steel SA 508 cl. 3 and stainless steel AISI 316L [6] according to the European standard. Three tests were performed at 20 and 300 °C for each base metal. The mean values of KCV are given in the table 4. Shear fracture appearance is equal to 0 % for all the tests.

θ°	20 °C	300 °C
Low alloy steel SA 508 cl.3	25 daJ/cm^2	32 daJ/cm^2
Stainless steel AISI 316L	35 daJ/cm^2	40 daJ/cm^2

Table 4: KV values for base metal

There is no significant effect of the specimen location in depth of the pipes.

Impact notch tests with specimen of Charpy V-notch type were carried out in the stainless steel buttering, with the notch located at 1.5 mm from the fusion line (that is in the first layer). The notch was oriented so that propagation of the break was radial, parallel to the fusion line. Due to the orientation and the lack of material to cut the specimen in the block, a build-up was performed by welding with nickel base alloy covered electrode (Fig. 17). The impact notch tests were carried out at different temperatures between – 40 and 300 °C.

The transition curve is shown in Fig. 18. In all cases, notch impact toughness specimens tested at or higher than 20 °C gave ductile tearing with fracture energy in excess of 40 J. The apparent transition observed for temperature down to 20 °C is typical of austenitic-ferritic welds.

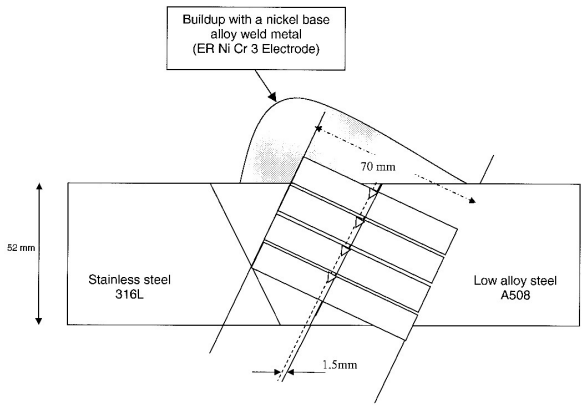

Figure 17: Charpy V specimen orientation

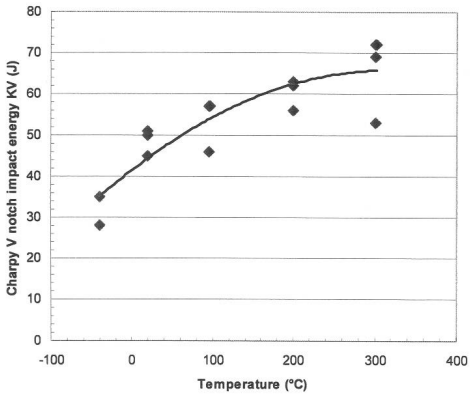

Figure 18: Charpy V impact toughness in stainless steel buttering with notch at 1.5 mm from the fusion line

CTJE25 specimens (Fig. 19) were pre-cracked by fatigue at room temperature /2/, at a maximum stress intensity factor of 25 MPa√m, for a/W = 0.5 (targeted) and then side grooved to ensure a straight crack front. In order to produce also nearly straight fatigue pre-crack front, the side-grooving operation was started prior to the pre-cracking (depth of groove = 0.032 B with B = specimen's thickness) and completed to a final depth of 10 % wall thickness after that.

The total length of the crack obtained was between 0.59 and 0.65 W. In each specimen, the fatigue crack growth deviated from the line of the notch at an angle of 25 to 33°, veering away from the fusion line and further into the buttering. Then, in some cases, the crack grew straight in the first layer and in other cases, grew until the interface between the second and third layers.

The corresponding J-R curves were obtained at 20 and 300 °C, using multiple specimens (interrupted tests); two tests were carried out by the single specimen compliance technique (partial unloading) at 300 °C. For these two specimens, there was good agreement between determination of the final crack extension by compliance and by optical measurements. The results are presented in Table 5 and Fig. 20 [6].

Test	$J_{0.2}$ (kJ/m^2)	dJ/da (MPa)	$J_{0.5}$ (kJ/m^2)	J_1 (kJ/m^2)
Single specimen	156	148	194	277
Multiple specimen	178	108	205	267

Table 5: J-R curve at 300 °C in the buttering at 1.5 mm from the fusion line

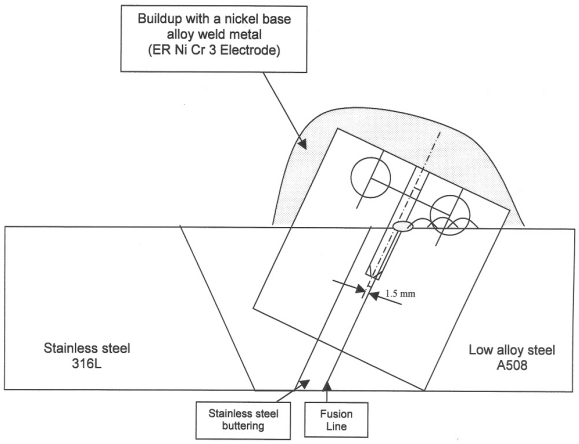

Figure 19: CTJE25 specimen orientation in stainless steel buttering at 1.5 mm from the fusion line

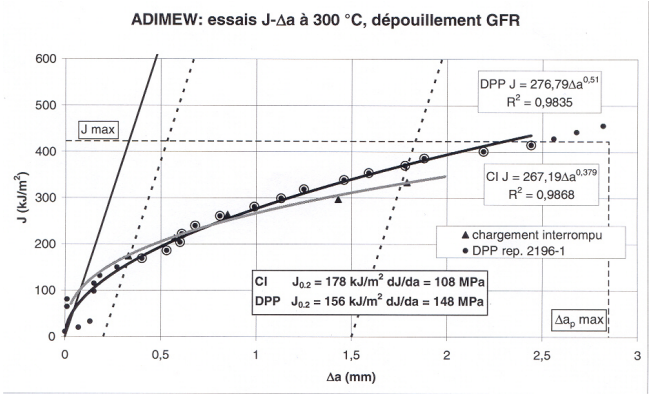

Figure 20: J-R curve at 300 °C for buttering with blunting line and offset line

Complementary toughness values of the buttering from SENB specimen

12 SENB tests were done at 300 °C, around the buttering layers [7]. The test results are presented in Table 6 and Fig. 21.

Specimen identity	Dimensions B, W, L	Notch location	$J_{0.2BL}$	$J_{0.5}$	$J_{1.0}$	$J_{2.0}$
	mm		kJ/m^2	kJ/m^2	kJ/m^2	kJ/m^2
A2-2(M2-2) A3-3(M2-3)	10, 10, 55	BU_{FL}	58 53	106 116	179 232	302 464
A2-3 A3-1	10, 10, 55	FL_{BU}	50 62	90 92	140 119	206 147
A3-2	10, 10, 55	CGHAZ	137	160	185	209
W01-01 W01-02 W01-03	10, 10, 55	WM	153 152 180	237 223 234	354 306 351	480 391 535
W01-04 W01-05	20, 40, 100	BU_{FL}	63 59	110 109	172 152	265 197

Table 6: SENB toughness results

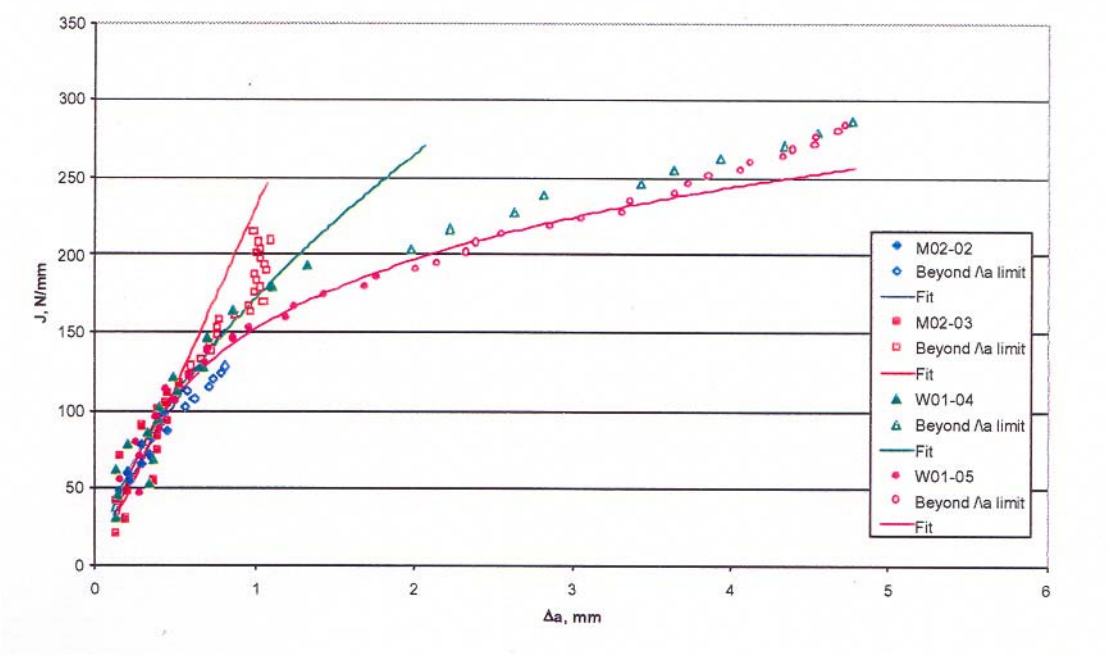

Figure 21: J-R curve results obtained for the buttering at 300 °C

Complementary toughness values of the buttering from notched CT specimen

In order to compare toughness level on fatigue pre-cracked and notched CT specimen, 5 CT tests were performed [8]. Test results are presented in Table 7 and Fig. 22.

Spec. No.	Notch radius, mm (as planned)	Defect distance, mm (as planned)	T, °C	C_1	C_2	J_{Ic}, kN/m
1	0.1	2	300	252.17	0.18	221
2	0.2	2	300	309.81	0.25	266
4	0.2	1	300	144.54	0.11	130
5	0.2	2	20	393.01	0.21	345

Table 7: Toughness evaluation of the buttering close to the fusion line from a notched CT specimen

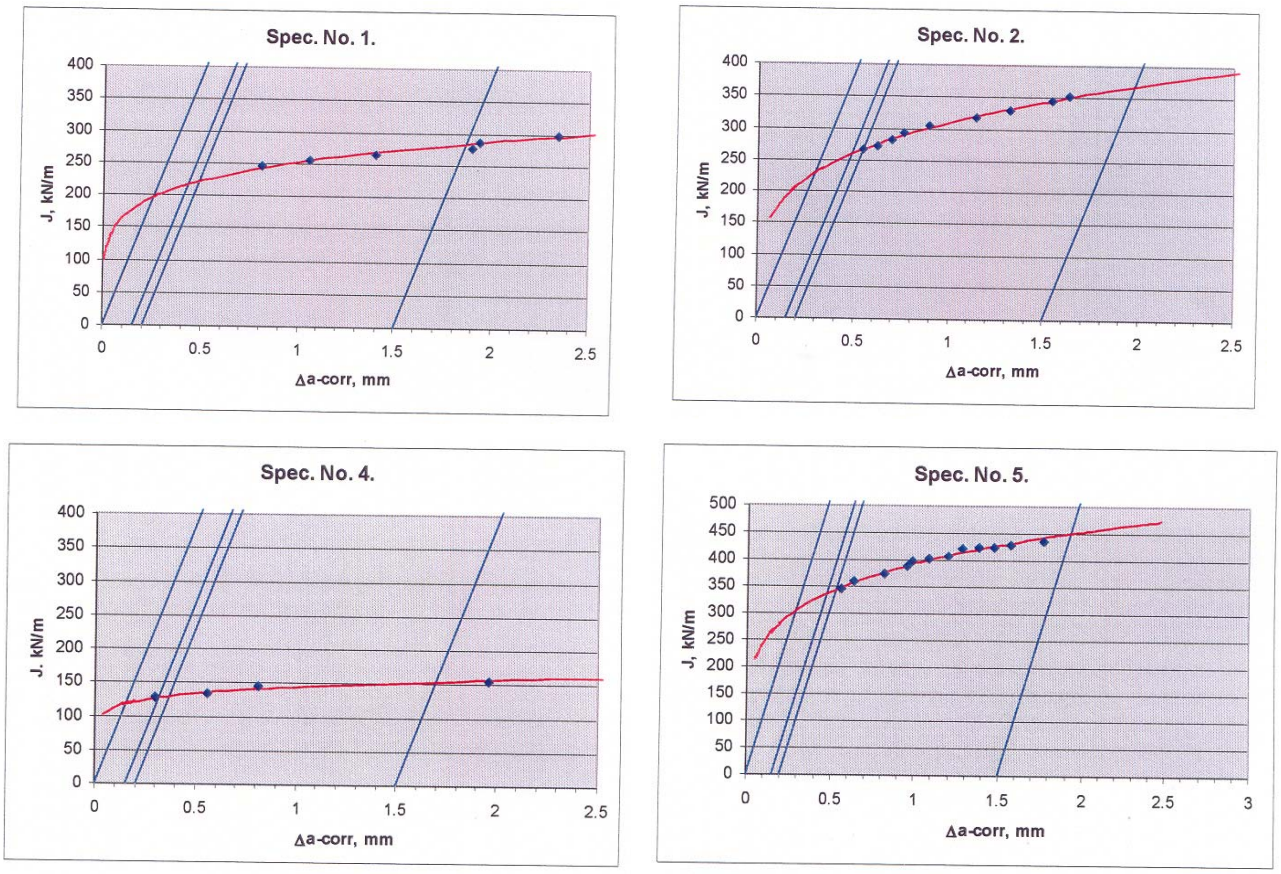

Figure 22: J-R curves obtained for the four different specimens

Complementary toughness evaluation on mixed-mode specimen

Fracture toughness testing under prominent mode II loading was conducted at ambient temperature. The tests were performed using multi-specimen techniques to evaluate the mixed-mode behaviour and implications of asymmetric loading to integrity of bimetallic welds. Single-edge notched bend specimens were tested at two configurations, cracks located 0.5 mm in BU from FL and 1.5 mm from FL in BU, respectively. Initial analyses illustrate the fracture toughness of the BU region being the lower the closer the FL the specimens have been sectioned. The experimental raw data is presented in [9].

Conclusion on buttering toughness and result transferability to different specimen or structure

The main feature of the results suggests that the buttering material on and near the fusion line of the ADIMEW dissimilar metal weld has a low $J_{0.2}$ initiation toughness and a low resistance to tearing. These are significantly lower than those of the bulk weld metal or the coarse grain heat affected zone. The buttering material on and near the fusion line is therefore the weld material with the lowest resistance to fracture. The $J_{0.2}$ obtained at 300 °C (55/54kJ/m2 from 10 x 10 mm specimens and 64/67 kJ/m2 from 20mm x 40mm specimens) are significantly lower than was obtained for equivalent buttering material in BIMET (120 kJ/m2). They are also lower than the values reference [6] and [8] obtained from compact tension tests of the ADIMEW weld. However, these tests indicated a flat R curve and comparable values at larger amounts of growth.

The reasons for the difference between ADIMEW and BIMET results are not entirely clear. It can be observed that the ADIMEW and BIMET welds were produced by different fabricators, although they were of comparable specification. Any differences in the detail of the welding procedure, consumables, thickness and heat treatment could be relevant. Examination of the relevant

microstructures of the BIMET and ADIMEW welds could determine if there were any significant differences between the weld materials.

GKSS and VTT undertook the BIMET fracture tests, and there could have been differences in the testing procedures and analysis methods that they used compared to those that TWI used.

Reasons for the differences with the [6] and [8] compact tension data are probably a result of differences in the notch and crack growth path rather than due to differences in specimen geometry. In the two single-specimen CT tests, the ductile crack growth deviated out of the side-groove and exhibited considerable tunnelling with the centre of the crack running well in advance of the edges. Both of these effects would tend to result in an overestimate of J compared with the TWI tests. In addition, [6] used a blunting line with a slope of 4 times the flow stress, giving a slightly lower slope than the $3.75R_m$ value that [7] used and hence a larger value of $J_{0.2}$. The [8] CT tests were undertaken on specimens with electro-discharged machined notches without fatigue pre-cracking, similar to the notch cut into the ADIMEW test weld. A higher value of $J_{0.2}$ relative to that obtained from fatigue pre-cracked specimens was therefore expected and observed. The [8] tests also showed some sensitivity of the R curve to the distance of the notch from the fusion line; with the toughness decreasing as the fusion line was approached on the buttering side. Differences in the positioning of the starter notch and fatigue pre-crack between the specimens could therefore also be a factor in explaining the differences between the R curves obtained. Measurement of the distance of the fatigue pre-crack and subsequent growth relative to the fusion line of each specimen could provide additional information in this respect.

The initiation value obtained for the CGHAZ reflects the different material microstructure. The estimated initiation values for the bulk weld metal indicate much tougher material.

- Fracture resistance curves at ambient temperature indicated that the BU layer/FL adjacent the ferritic HAZ possesses the lowest fracture resistance. Crack propagation resistance is particularly low.
- The obtained values of $J_{0.2}$ for the buttering material show scatter. Possible reasons could be due to differences in the mode of growth, testing and analysis procedures, the distance of the crack from the fusion line, and the effect of notch/crack sharpness.
- The values of J for the buttering material that the three laboratories obtained at 1 and 2 mm of tearing are more consistent, and show that significant growth in this material is possible with a minimal increase in load.
- The estimated initiation values for the bulk weld metal and coarse grain heat affected zone indicate much tougher material.
- The flow and uniaxial true stress-strain curves are nearly identical for austenitic regions due to large deformations and hardening associated with necking. In these cases the better curve fit is recommended over the theoretically valid one.
- For ferritic A508 the deformation behaviour during necking tends towards higher curvatures due to smaller hardening. In these cases the differences between the Hollomon and Ramberg-Osgood stress-strain curves are large enough to cause large evaluation errors if the Hollomon expression is used at strain ranges exceeding necking.

If further work were to be considered, then it is recommended that the following would add value to the results already obtained.

- Determination of a more exact value of the h factor that should be used in the computation of J for the ADIMEW dissimilar metal weld specimens and re-analysis of the R curves using this value.
- More detailed examination of the relevant microstructures in order to investigate why the initiation toughness of the ADMEW buttering material is much lower than that of the bulk weld metal and that obtained for equivalent buttering material in the BIMET study.
- More detailed comparison with the results obtained by partners taking account of the mode of growth, testing and analysis procedures, the distance of the crack from the fusion line, and the effect of notch/crack sharpness.

1.3. Residual stresses

Dissimilar metal welds between ferritic and austenitic steels exhibit a strong residual stress field, both as welded and after PWHT (post welded heat treatment). Knowledge of the residual stress is an important input to the structural integrity analysis of DMWs. The residual stresses have been measured non-destructively and through thickness by means of neutron diffraction. Some complementary checks have been done with the hole drilling technique. Different computation have been checked and compared with the measurement results.

Measurements by neutron diffraction technique

Neutron diffraction is a powerful tool for non-destructive determination of residual stresses, deep within crystalline materials at reasonable spatial resolution. At the high-flux reactor (HFR) of the JRC there are two facilities dedicated to this test method. One of them is the Large Component Neutron Diffraction Facility (LCNDF), where the ADIMEW specimen has been tested [10].

In order to fit on the LCNDF, AD01 had to be shortened to an overall length of 500 mm and on both ends a particular sector had to be removed additionally, to facilitate access of the neutron diaphragms. Finally a “window” had to be cut across the weld to allow for neutron beam access, when measurements in hoop direction were to be made. Hence, in total three parts have been removed (Fig. 23 to 25) in order to facilitate the neutron diffraction measurements. Both edge sectors were removed by milling, while the central “window” was removed by spark erosion. During spark eroding the “window” surface strain development was monitored by strain gauges, in order to provide an estimate of the stress relief caused by cutting. The results demonstrated that hardly any stress relief occurred at the location foreseen for neutron diffraction measurements (about 105° from the window). This justified the assumption that measurements in a component prepared as described would still reflect very well the original stress state.

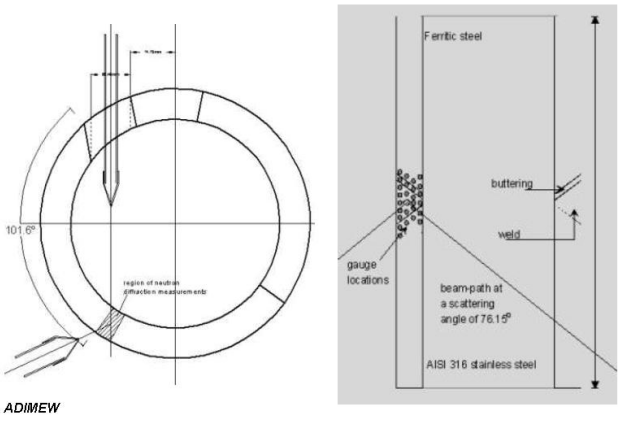

Figure 23: Set-up for neutron diffraction measurements

Figure 24: Residual stress measurement on AD01

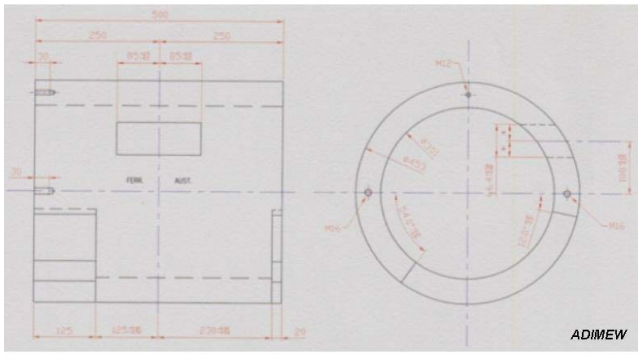

Figure 25: Overview of "windows" removed from AD01 mock-up

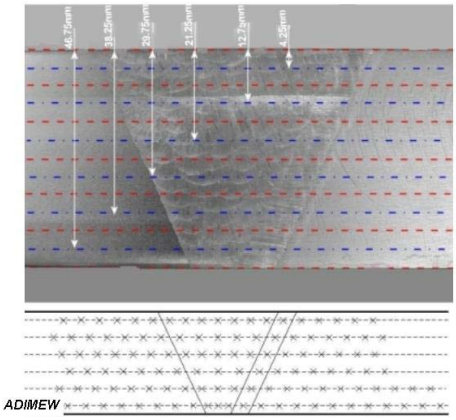

Figure 26: Neutron diffraction measurement locations

A 10 mm radial slice was wire eroded from the “window” cut-out, to provide small "coupons" of appropriate dimensions for the estimation of the stress free (reference) lattice distance at all intended test locations. The thickness of the slice has been measured to be 51 mm, which means that the groove sides are inclined at approximately 25^{o}. In order to facilitate complete relief of residual stresses the slice was subsequently cut into two pieces along the buttering ferrite interface, and then a structured grid of cuts was applied to each of the two pieces, which left only the parallelepiped-shaped coupons (~ $9 \cdot 8.5 \cdot 10$ mm^3) intact.

Measurements were performed at various locations within the weld, the buttering layer and base materials in three orthogonal directions, i.e., the component hoop, axial and radial directions. The locations, where measurements were made, are shown in Fig 26. They were on six axial lines uniformly distributed across the specimen thickness, i.e. 4.25, 12.75, 21.25, 29.75, 38.25, and 46.75 mm from the external surface of the pipe.

Fig. 27 to 29 present the measured axial, radial and hoop strain and stress distributions, respectively, along the axial direction of the pipe, at 6 distances from its outer surface. These results show that while strain estimates in the hoop direction are of excellent quality throughout the entire material specimen domain examined, the radial and axial strain data are of inferior quality. This is due to material texture, which favours diffraction testing in the hoop direction at the expense of the radial and axial directions.

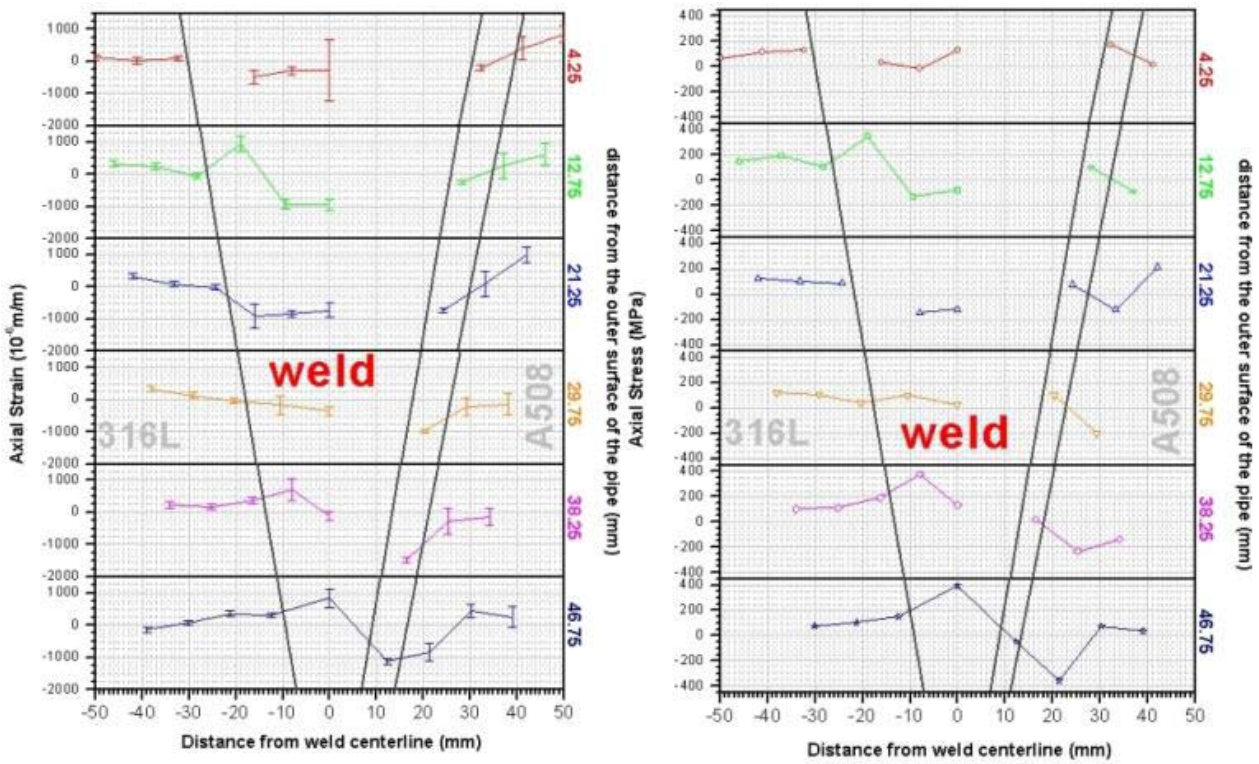

ADIMEW

Figure 27: Axial strain and stress measurement results

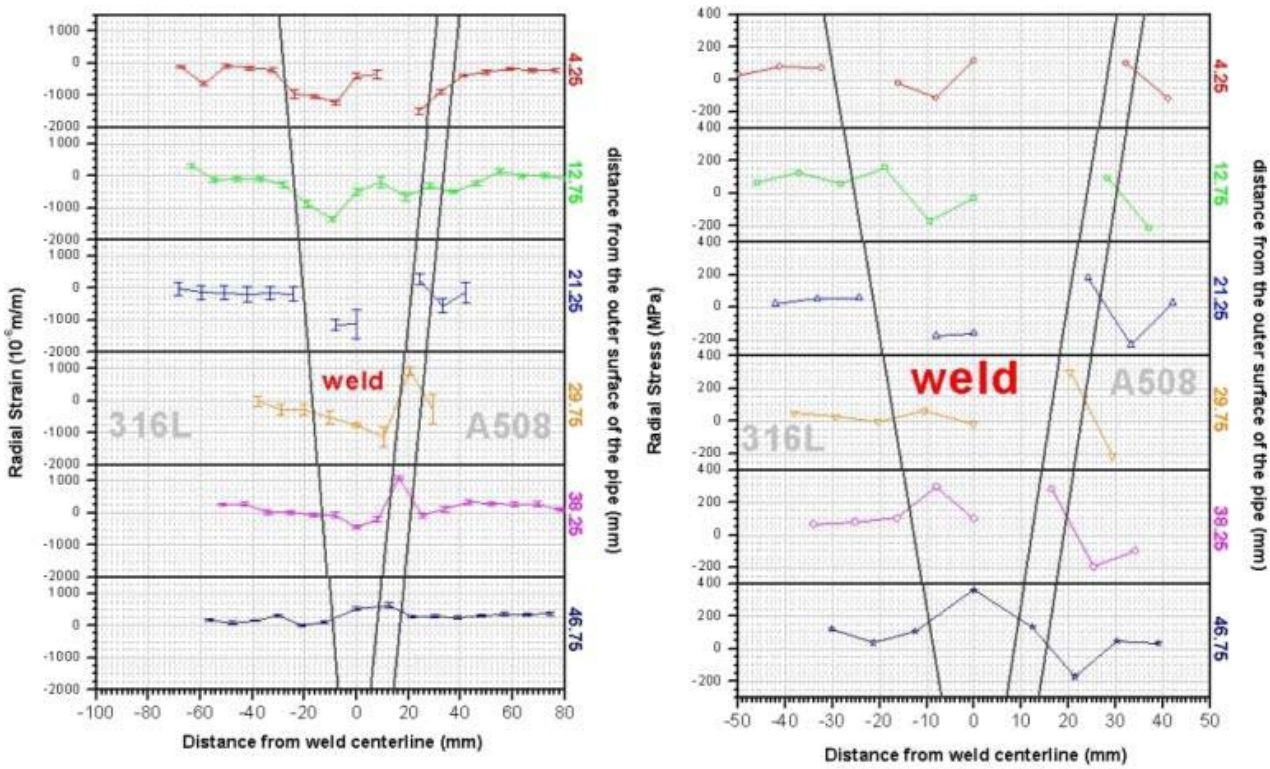

ADIMEW

Figure 28: Radial strain and stress measurement results

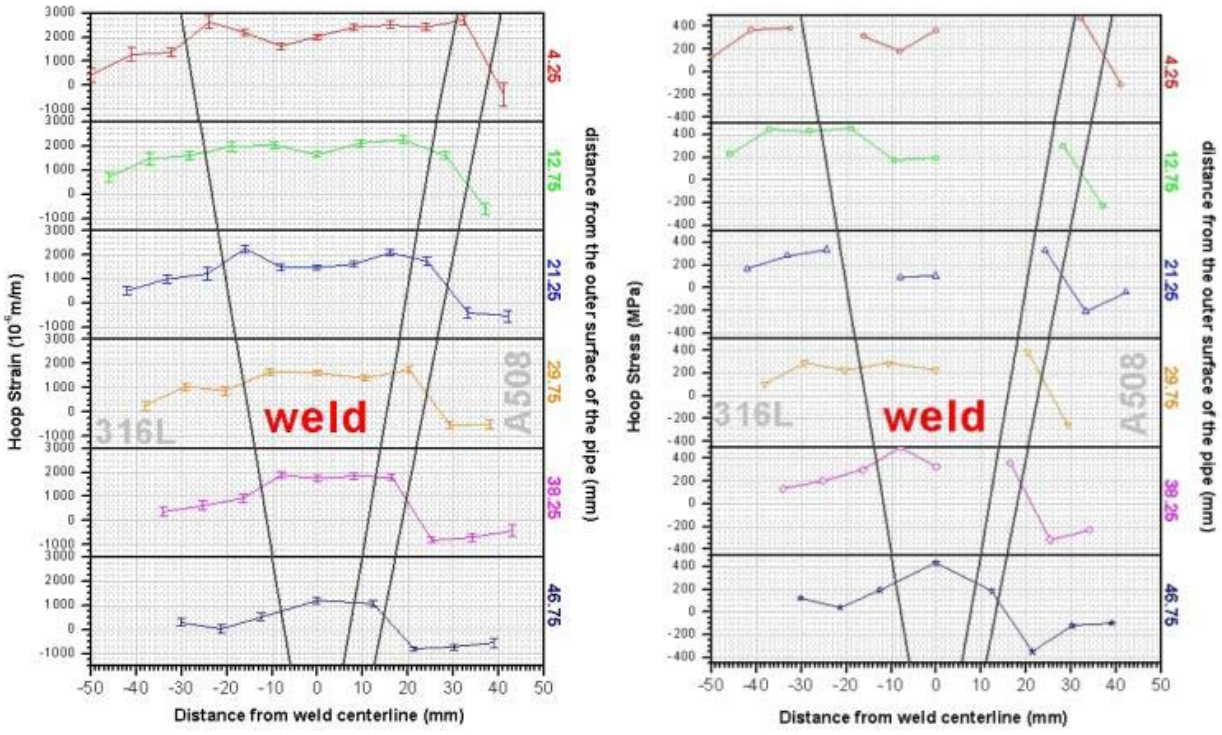

Figure 29: Hoop strain and stress measurement results

Complementary measurements by drilling-hole technique

Using the surface hole drilling method, measurements have been made at ten locations on the outer surface of the pipe and at four locations on the inner surface in the vicinity of the austenitic weld buttering to ferritic pipe fusion boundary [11]. The locations of the measurements relative to the weld fusion line with the A508 pipe, at the outer or inner surfaces as appropriate, and the circumferential 0^o datum (as inscribed along the length of the pipe) are shown in Fig. 30 (a) and (b). The co-ordinate positions are tabulated in Table 1 using x-y axis (x for circumferential and y for axial directions), together with the type of material sampled.

The results are presented on Fig. 31 and 32.

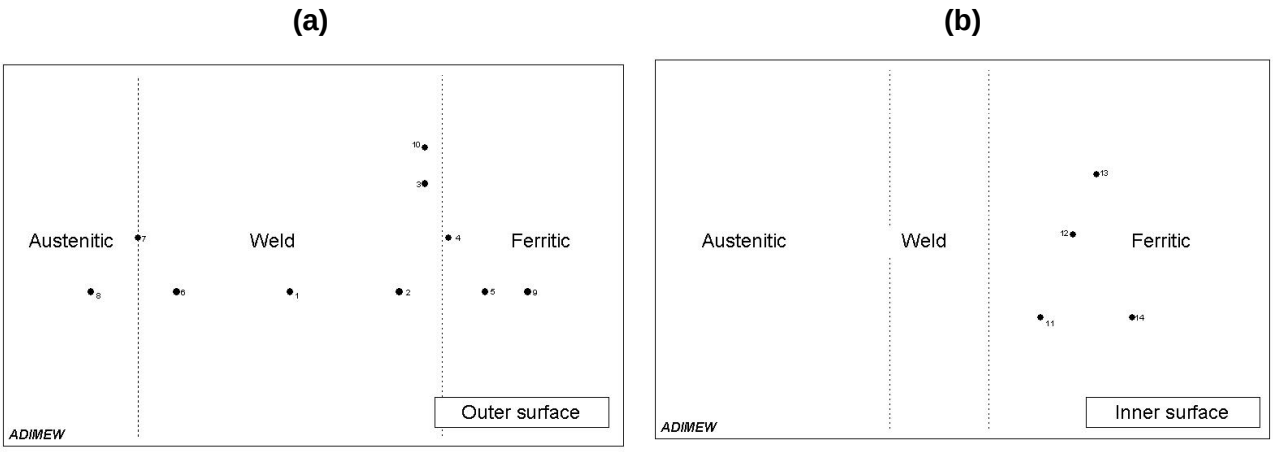

Figure 30: Residual stress measurement locations (a) on the outside, (b) on the inside of the pipe

Gauge N°	x, mm	y, mm	Depth, mm	Diameter, mm	Calibration constant	Strain 1	Strain 2	Strain 3	Material
1	35.5	40	2.21	2.032	2.727	340	168	-128	308
2	10	40	2.16	2.042	2.702	388	256	-116	308
3	4	70	2.03	2.125	2.509	291	243	52	308
4	-1.5	55	2.08	1.996	2.818	-21	150	220	A508
5	-10	40	2.11	2.017	2.765	24	173	183	A508
6	62	40	2.13	2.076	2.619	214	137	-123	308
7	71	55	2.26	2.069	2.637	395	153	-78	308
8	82	40	2.11	2.078	2.616	324	206	40	316
9	-20	40	2.06	2.061	2.655	49	153	180	A508
10	4	80	1.98	2.038	2.711	232	256	65	308
11	11.7	31	2.00	2.073	2.628	16	191	337	A508
12	4	54.2	2.00	2.102	2.560	5	305	637	A508
13	-1.5	71	2.00	2.151	2.452	402	161	540	A508
14	-10	31	2.00	2.078	2.617	292	138	26	A508

Table 8: Gauge locations, hole size and strain measurements

Gauge	Maximum principal stress MPa	Minimum principal stress MPa	Axial stress (x) MPa	Circumferential stress (y) MPa	Theta °
1	19	-184	-181	16	97
2	11	-221	-210	0	103
3	-69	-177	-169	-77	105
4	-24	-142	-29	-137	-11
5	-38	-131	-50	-120	-21
6	43	-111	-102	34	104
7	-23	-215	-215	-23	89
8	-78	-194	-193	-79	95
9	-58	-122	-62	-118	-15
10	-58	-172	-150	-80	116
11	-67	-198	-68	-197	-3
12	-110	-359	-110	-359	1
13	-217	-465	-315	-368	39
14	-67	-179	-178	-68	86

Table 9: Axial and circumferential stresses at each gauge location

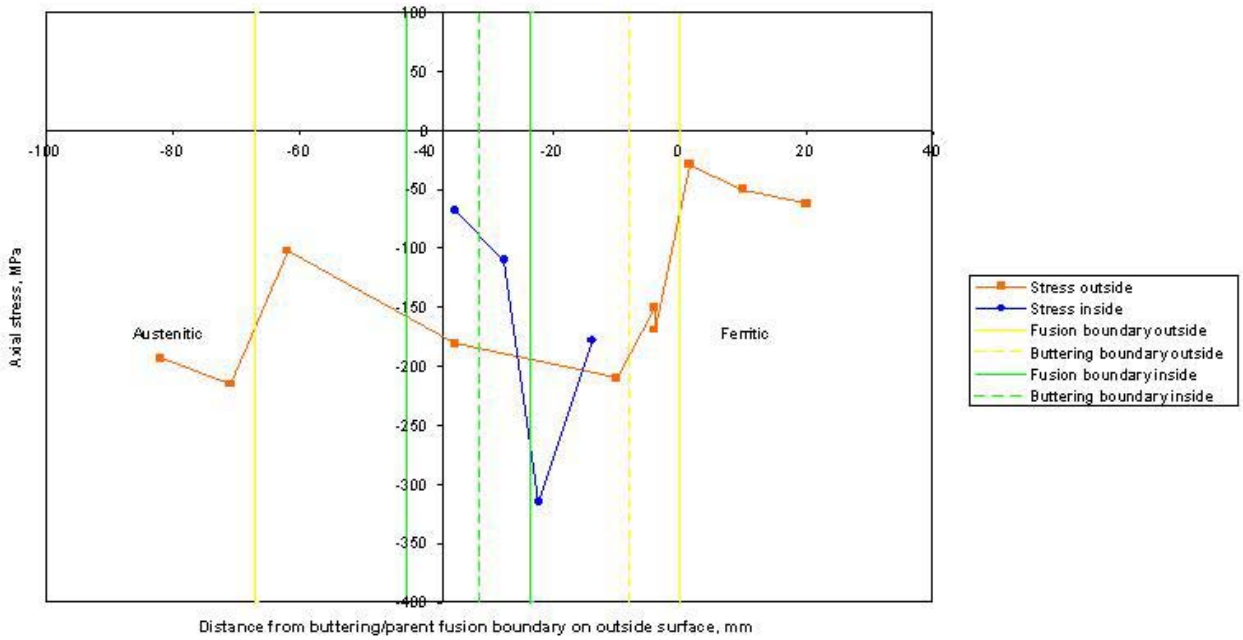

ADIMEW

Figure 31: Axial residual surface stresses

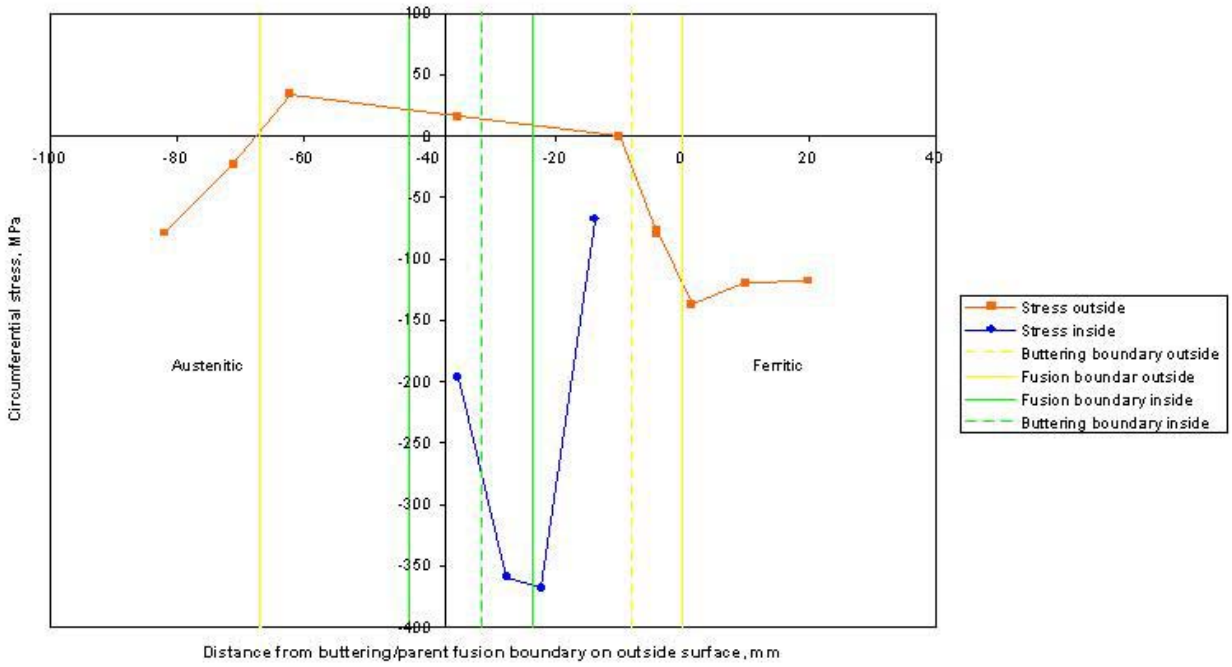

ADIMEW

Figure 32: Circumferential residual surface stresses

Residual stress modelling

The modelling task involves the evaluation of the residual stress field using different modelisation types [12]. The two following calculations have been performed on 2D axi-symmetric geometry:

- a simplified analysis, which consists in a cooling calculation from an assumed stress-free state (600 °C for AD01) after the stress-relief heat treatment
- a detailed analysis, which simulates each elementary step of the mock-up manufacturing procedure, from buttering stage to final machining after PWHT stage.

Material characteristics

Three materials are considered: A508 for ferritic base metal, 316L for austenitic base metal, and 308L for weld metal. The buttering was considered as identical to the filler weld material in the present study. Fig. 33 shows the different zones of material.

The yield limit $R_{e0.2\%}$ and stress-strain curves at 20 and 300 °C from ADIMEW material property report has been used (Table11). The RCC-M code [13] has been used for the materials database for current temperatures. These data were extrapolated using private database and referring to past Framatome-ANP similar analyses.

	$R_{e0.2\%}$ (Mpa)		
Temperature (°C)	A508	316L	Weld metal (WM)
20	494	254	318
300	454	182	196

Table 10: Yield limit of the different materials

In the detailed analysis, creep characteristics have been taken into account during PWHT stage.

The HAZ is hardened during the welding process trough a complex process that needs to model metallurgic transformations in the ferritic steel. These processes have not been modelled. We used constant mechanical properties from the interface to HAZ half-depth (complete austenitisation) and then decreasing ones according to the depth, down-to-base metal values.

Stress-relieved mechanical properties were taken into account during PWHT simulation (both calculations).

Geometry

The mock-up geometry has been carefully checked. The dimensions of the pre- and post-final machining AD01 mock-up is defined in the manufacturing report and reported in Fig. 34.

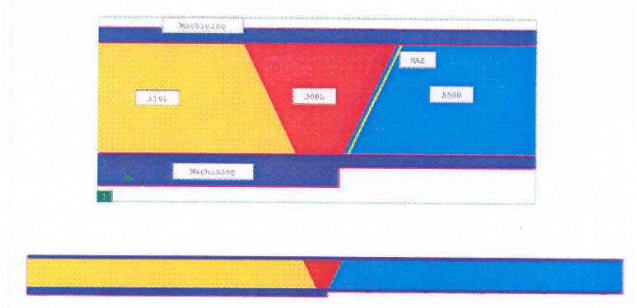

Figure 33: Material used in the models

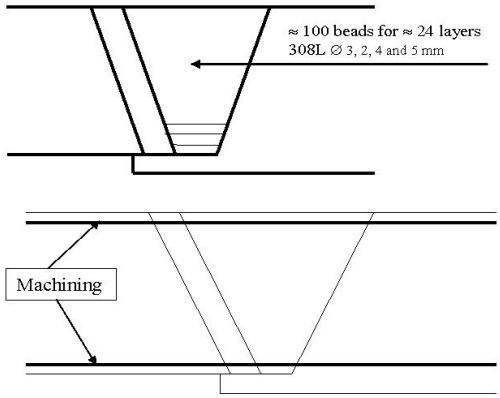

Figure 34: Machining of the mock-up used in the models

Finite-element model

A unique model, based on the pre-final machining AD01 mock-up geometry (length = 1040 mm) was used for the two types of analysis.

The model is 2D axi-symmetric. The self-restraint effect of the cold parts during welding is taken into account by appropriate boundary conditions: fixed-end displacement is applied during the heating phase and free boundary conditions during the cooling phase.

Only three buttering layers (1309L and 2308L) have been modelled, the fourth one was not considered. The joint is filled with 18 macro beads of 308L.

The mock-up is meshed using quadratic elements. The use of quadratic elements increases the size of the problem, but they give much better results than linear elements (for the same number of nodes) at locations where stress gradients are high like at the interfaces. The mesh contains 2980 2D quadratic elements and 9023 nodes.

Manufacturing and welding

The manufacturing process and the welding parameters used in the models are presented in Tables 12 and 13 respectively.

The machining is modelled making the element strength to vanish: the Young modulus is decreased to a very low value and Poisson ratio is set to zero. Only the removal of material and its consequences on stress redistribution is taken into account. The heating due to machining is neglected.

The two machinings have been modelled:

- machining of the buttering after post-heating (reduction of the third-layer thickness in the detailed analysis)
- final AD01 mock-up machining after PWHT (reduction of austenitic and ferritic section external and internal diameters in both simplified/detailed analyses).

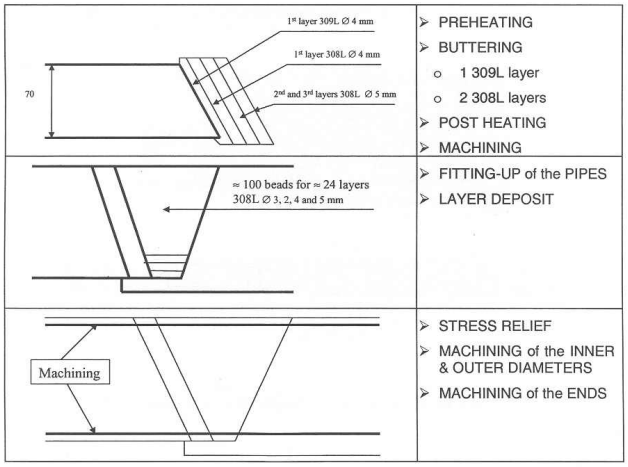

Table 11: Manufacturing used in the model

		Buttering	Welding
Preheating temperature		151°C	20°C
Amperage	Phi=4mm	90-160 A	115-145 A
	Phi=5mm	170-200 A	170-200 A
Voltage		24 V	24 V
Welding speed		20 cm/min	20 cm/min
Post weld treatment		Post heating 320°C – 4h15' (mean value)	PWHT 20°C->600°C – 40°C/h 600°C – 6h08' 600°C->20°C – 38°C/h
Machining		Post-PH	Post-PWHT

Table 12: Welding parameters

Simplified PWHT analysis

This analysis considers that the mock-up is stress-free at the post-weld heat treatment (PWHT) temperature (610 °C). The simulation reduces to the computation of cooling from PWHT temperature to room temperature. The residual stress fields are induced by the difference between thermal expansion coefficient values of the materials and by the final machining.

Detailed analysis

This analysis consists in simulating the AD01 mock-up entire manufacturing process, from buttering stage to final machining after PWHT stage. The welding parameters are those defined in the manufacturing report.

The "macro-bead" technique

The macro bead technique consists in modelling the welding operation by a deposit of layers of beads instead of a full sequence of bead deposit.

The technique is conducted under the small displacement hypothesis and assuming 2D axi-symmetry of the joint.

The main features of the technique are:

- One macro bead is defined per weld bead layer (3 for the buttering, 18 for the joint).
- Return to room or preheating temperature between two macro beads.
- In order to prevent from excessive distortions during macro bead deposit simulation, additional elements (vertical stiffness) are fixed on the top of the joint.
- The cyclic effects due to upper bead layers (overlapping of two successive bead layers) is restored through appropriate thermal conditions
  - One bead thermal cycle (heating up to fusion temperature to cooling down) is uniformly applied on the macro bead itself and on the associated re-melted zone too (~ 30 % of the melted metal total height).
  - One macro bead thermal conditions defined giving a "horizontal" stretch of the furthest bead thermal conditions: the material is considered as "fictional" between one layer furthest half-beads (nil thermal characteristics except horizontal thermal conductivity, which ensures temperature continuity between both "real"/"fictional" structures; isotherms in the "fictional" part are therefore parallel to the macro bead surface).

- Three specific thermal adjustments on a 3D model of the structure with one 360° weld bead:
- 1 for the buttering with preheating (151 °C; I = 140 A whatever the diameter).
- 2 for the joint without preheating (20 °C): 1 for the lower third of the joint (phi = 4 mm; I = 135 A) and 1 for the upper two third of the joint (phi = 5 mm; I = 185 A).
- These calculation results have been compared to residual stress measurements.

Modelling versus measurements comparison

The results are shown and compared together, for the two different models [12], Fig. 35 to 38, and to the experimental measurements on Fig. 39 to 42.

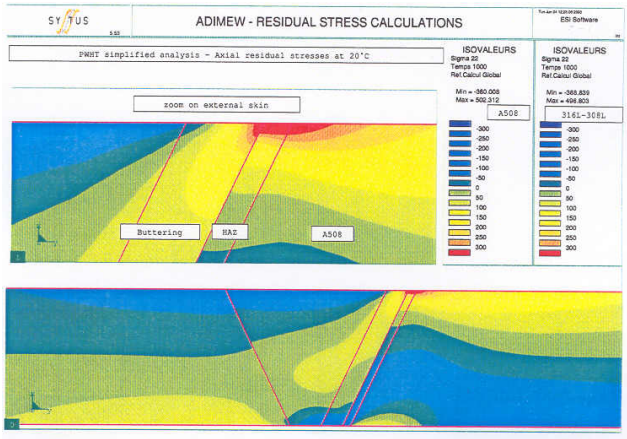

Figure 35: Simplified model – axial stresses

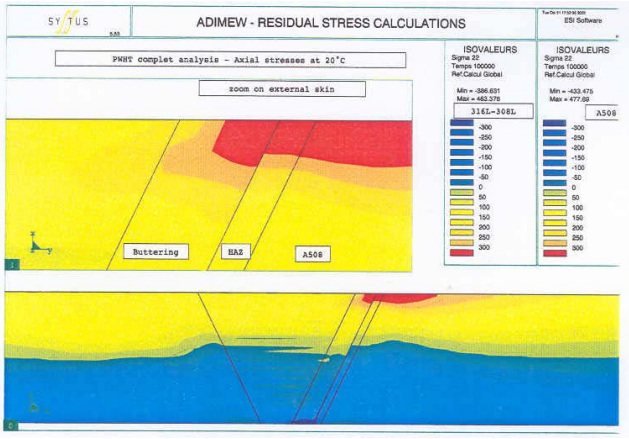

Figure 36: Detailed model – axial stresses

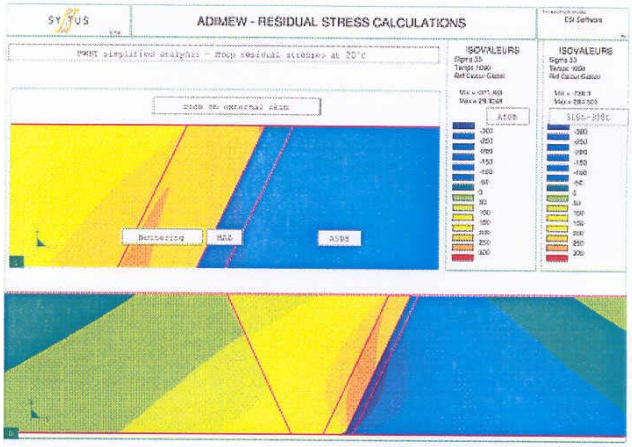

Figure 37: Simplified model – hoop stresses

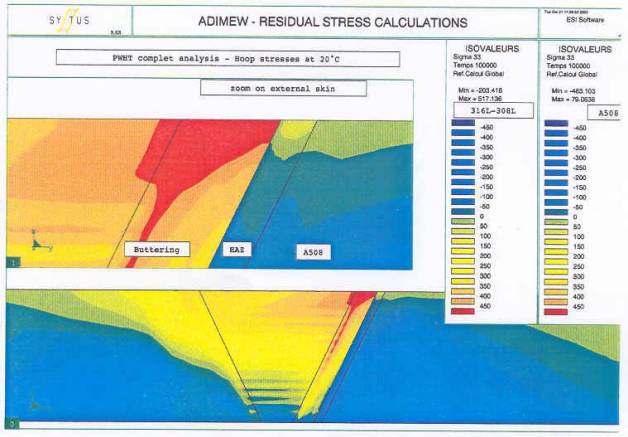

Figure 38: Detailed model – hoop stresses

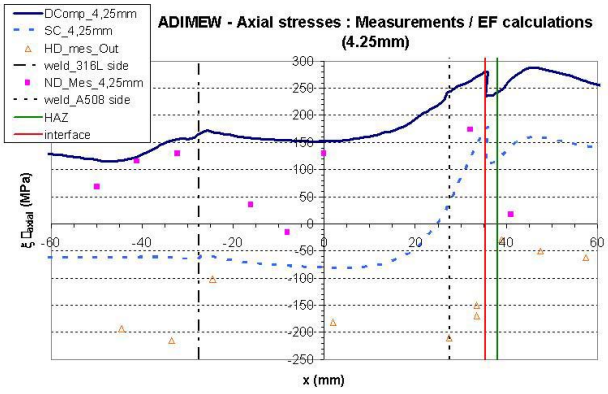

Figure 39: Comparison with measurements – 4.25 mm from outer surface

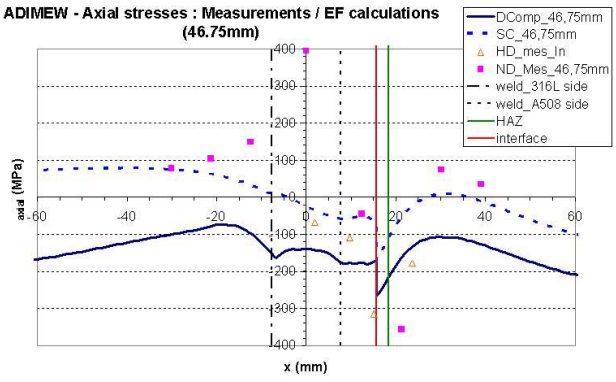

Figure 40: Comparison with measurements – 4.25 mm from inner surface

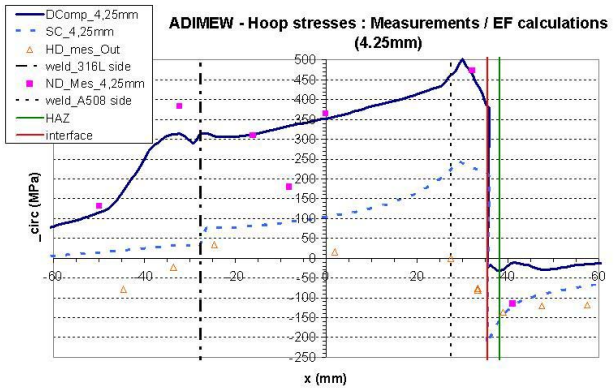

Figure 41: Comparison with measurements – 4.25 mm from outer surface

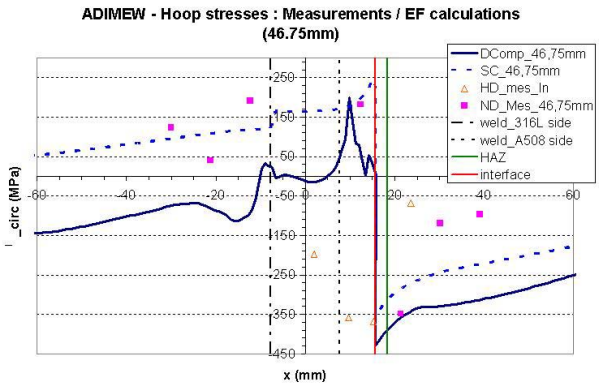

Figure 42: Comparison with measurements – 4.25 mm from inner surface

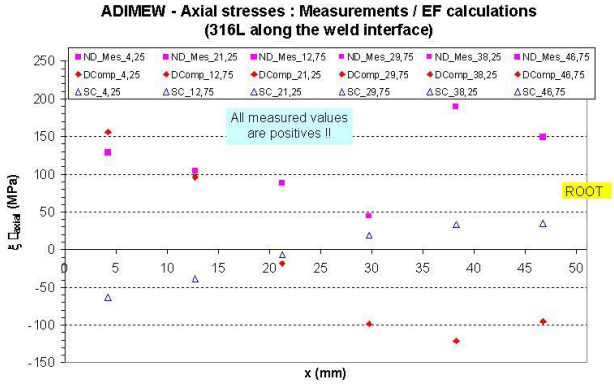

Figure 43: Comparison with measurements – along the fusion line

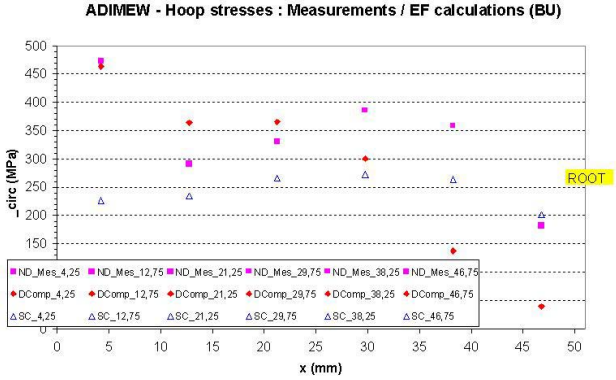

Figure 44: Comparison with measurements – in the buttering

Conclusion on residual stresses

- Large differences are observed on simplified and detailed computations.
- An excellent agreement is observed between the most reliable ND stress measurements and detailed computations, except in the vicinity of the root pass. We consider that these differences are due to a weakness of the "macro bead" technique when applied to the buttering.
- We attribute the differences between hole drilling measurements and extrapolation of ND measurements on the walls to machining. The heating due to machining may induce considerable compressive stress on a thin layer under the surface. This effect has not been modelled in the residual stress simulations.
- Tensile axial residual stresses are predicted along the crack location, therefore producing an increase of the crack driving force J.
- However, the residual stress fields are not likely to influence the crack initiation since the crack initiate when the ligament is fully yielded. A similar observation has been made on the smaller BIMET DMW.

1.4. Benchmark test

Test facility and mock-up installation

The mock-up, including its welded bending arms, has been tested under 4-point bending conditions at 300 °C, as foreseen in [14]. A testing installation has been adapted on purpose in order to perform this full-scale test at EDF-R&D. This installation looks like Fig. 45 and its principle is presented in Fig. 46.

Figure 45: Sight of the test installation SEM at EDF-R&D

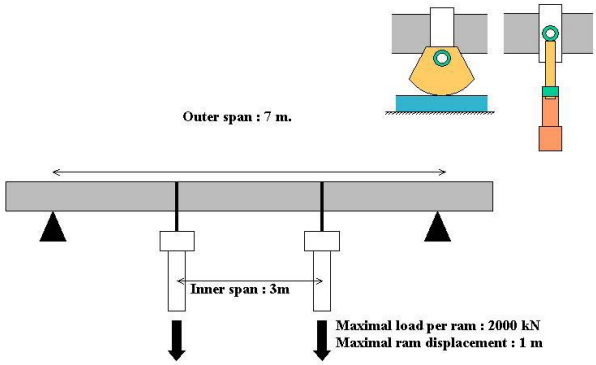

Figure 46: Principle of the test: scheme of the rig; supporting wheels; pulling crank arms

The test was conducted under displacement control (with a loading speed v = 0.3 mm/min), so that we could not assure that the rams forces would be equal: the problem was then that we could get a very high force on one side and almost none on the other one. We would then lose the advantage of 4-point bending conditions and also overcoming the allowed load on one ram. Therefore, we processed pre-test analyses [15] to optimise the position of the pipe on the rig in order to reach the forces equilibrium. The offset (as illustrated on Fig. 47) was set to 285 mm.

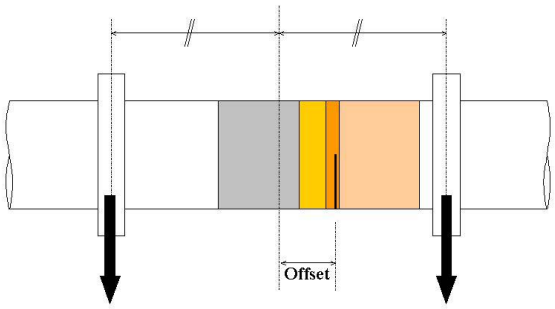

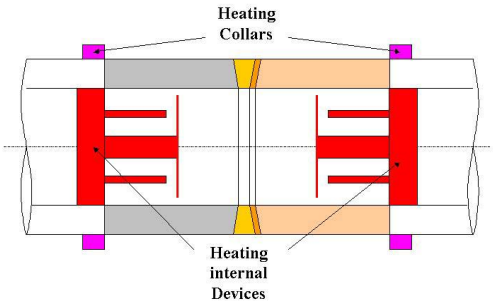

Figure 47: Illustration of the offset to reach the ram forces equilibrium

Figure 48: Heating system

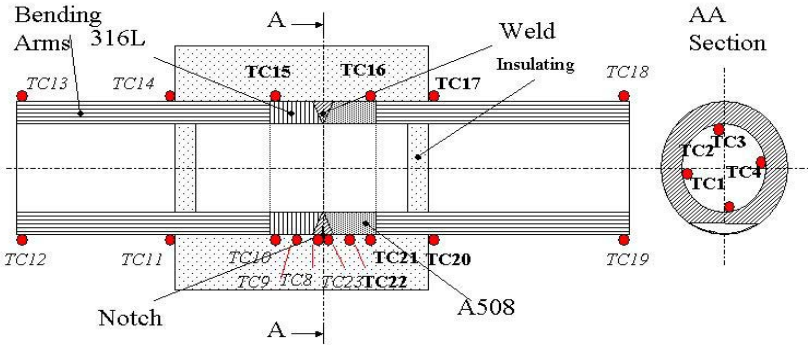

Figure 49: Thermal instrumentation

To reach 300 °C around the defect and to keep a reasonable temperature in the bending arms (to assure a fully elastic behaviour) we used a double heating system, as shown on Fig. 48. On the outer surface of the pipe were fixed heating collars, using the conduction mode, while other heating devices were installed inside the pipe, using radiation and convection modes. As all electric powers were adjustable, we could theoretically reach the aimed temperature field.

Mock-up instrumentation

In order to measure this field [17], thermocouples had been installed all around and inside the pipe (Fig. 49). Unfortunately one device did rapidly break out. The temperature field looked like on Fig. 50 during the test. This temperature field remained stable during the test, as can be seen on Fig. 51: There is only an increase of around 3 °C between the beginning and the end of the test. With this heating system, we could not avoid a vertical gradient (about 23 °C) between the top and the bottom of the pipe.

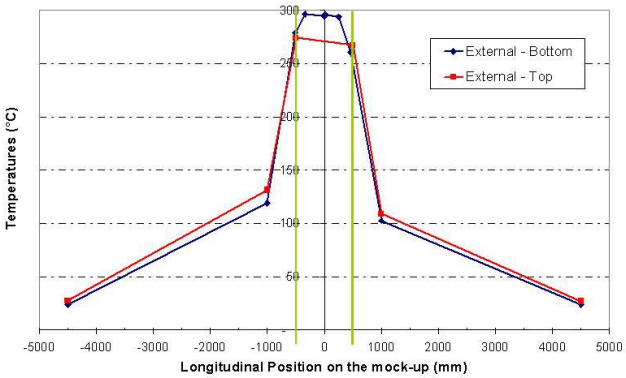

Figure 50: Longitudinal thermal profile of the pipe

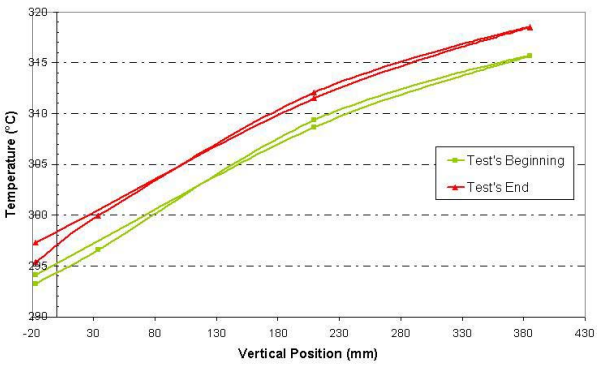

Figure 51: Vertical thermal profile in the defect's section

We also installed mechanical instrumentation [17] [21]:

- to control the testing conditions:
  - clinometers to quantify the rotations of the collars and crank arms;
  - extensometers to measure the gliding between the pipe and the collars used to transmit the load;
  - strain gauges on the crank-arms, to verify that the load is symmetric and that the crank arms remain elastic all along the test
- to observe the global mechanical behaviour of the pipe, we used different captors:
  - rope captors to measure the rams displacements and the pipe's deflection;
  - clinometers to get an idea of the curvature of the pipe during the test;
  - extensometers to observe the pipe's ovalisation;
  - strain gauges to know the strains at different locations of the pipe
- to characterise the fracture behaviour of the structure:
  - electric potential measurements, to determine the instant of crack initiation;
  - knife captors to measure the crack mouth opening displacement at five different locations of the defect;
  - extensometers, to reach the crack mouth opening angle in the middle of the defect.

We measured also the force transmitted through each ram during the entire test.

We proceeded as mentioned in [18] and there has been no major problem during the test, which lasted around 2 hours, on 23 July 2003 [20]. The main results are provided in this synthesis report and are completed in [21].

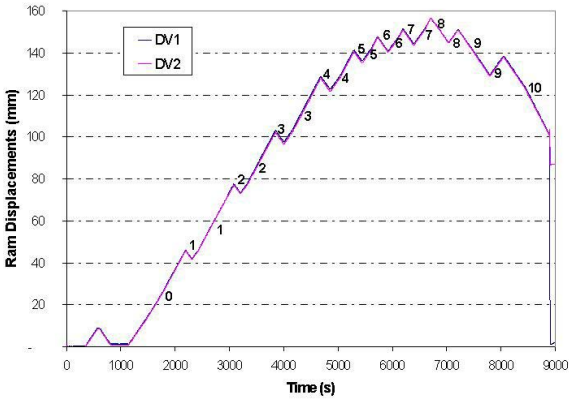

Figure 52: Evolution of corrected rams displacements against the time

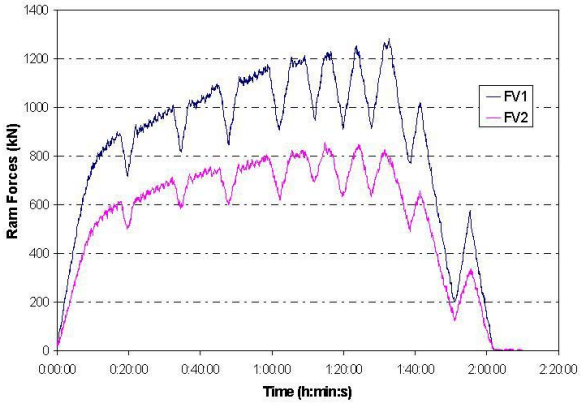

Figure 53: Evolution of rams forces against the time

Concerning the rams displacements, they have been corrected, taking into account the crank-arms elongation we measured through the strain gauges fixed on them. The rams displacements are not perfectly the same (even if it looks like on Fig. 52): the maximal difference is about 2.8 mm at its maximum, which is less than 5 % of the average ram displacement. This could look like insignificant, but its consequences are huge and can be seen on Fig. 53: the ram force we registered on the austenitic side is permanently about 40 % higher than the other one. Some post-test analyses showed [19] that this difference could be completely explained by this delay of the ferritic ram displacement.

Test conduction and results

The global response of the structure to the bending load can be summarised by the load-displacement curve. As we have two rams, there are two such curves (which are presented on Fig. 54) in our case. Some hydraulic regulation problems leaded to the halting aspect of these curves, what can be erased plotting the bending moment (calculated at the initial position of the crack tip and assuming small rotations) against the average ram displacement.

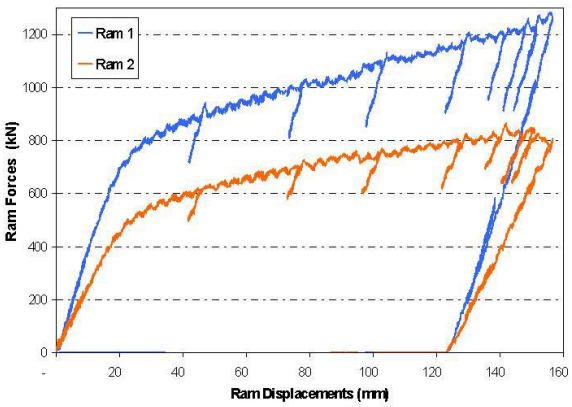

Figure 54: Evolution of rams forces against the corrected rams displacements

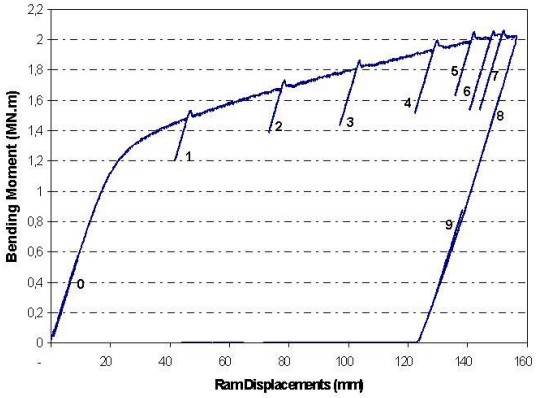

Figure 55: Evolution of bending moment against the corrected average ram displacements

Rotations and deflections are plotted against the time respectively on Fig. 56 and 57. These figures indicate that the pipe's global deformation remained approximately symmetric to the defect's section.

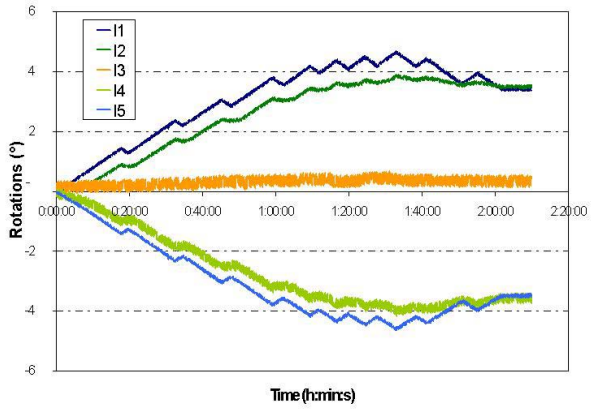

Figure 56: Evolution of rotations against the time

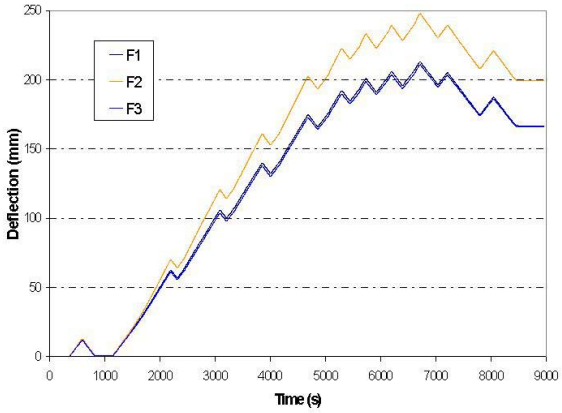

Figure 57: Evolution of deflections against the time

To determine the instant when the crack initiated, we can use different methods. The most common one is to use the electric potential (EP) method. Observing the EP against ram displacement (Fig. 58), we can determine the initiation instant, when a sudden change of slope occurs. This leads to a crack initiation for a ram displacement around 126 mm.

Another method consists in observing the CMOD: any acceleration in the CMOD/ram displacement curve corresponds to crack propagation. Looking carefully to this curve we can identify two types of accelerations:

- After each unloading/reloading period (from the second one), there is a tiny acceleration; these accelerations are due to the small overload that appears after each reloading.
- When considering the global shape of this curve, we can identify a tiny acceleration approximately at the same moment; a very large acceleration of CMOD occurs at an average ram displacement around 140 mm: this corresponds to a very large and quick crack propagation.

The average ram displacement at the crack initiation instant determined through CMOD is then around 115 mm.

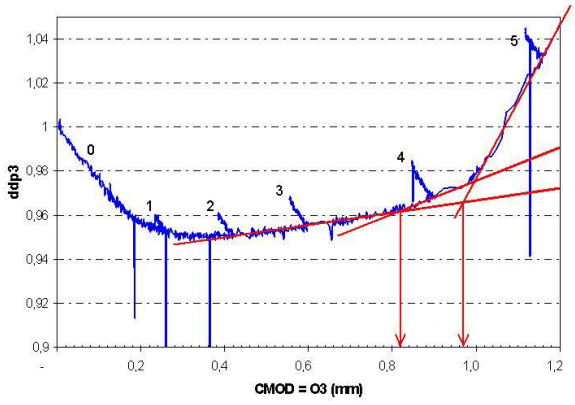

Figure 58: Evolution of electric potential against CMOD

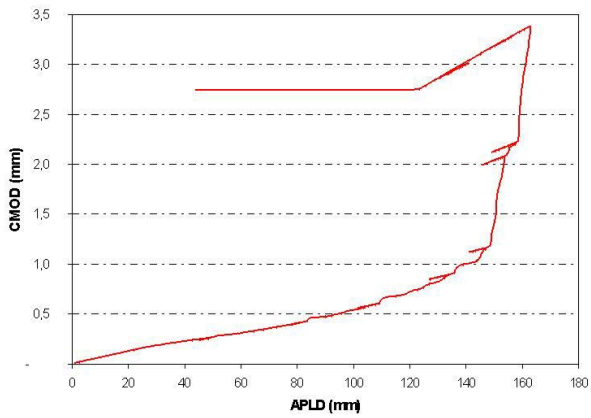

Figure 59: Evolution of CMOD against average ram displacement

Other approaches (exposed in [21]) can be used, like the compliance method, which gives information about the crack propagation. This can also provide an interval in which the crack initiated (actually 78-103 mm). We also performed a more complicated method mixing the compliance method with the EPM. This leads to a different result. This is also the case if we use

the crack mouth opening angle (and the displacement of the “rotation centre” of the crack opening process). All the results are consigned in Table 13.

	CMOD (mm)	APLD (mm)	Bending moment (MN.m)	Ram #1 force (kN)	Ram #2 force (kN)
EPM	0.83	126	1.91	1144	795
CMOD	0.72	115	1,86	1123	769
Compliance	0.42-0.59	78-103	1.70-1.79	1026-1078	703-744
Mixed approach	0.82	125	1.91	1152	787
CMOA	1.00	135	1.96	1179	810

Table 13: Crack initiation results

All these data provide an interval in which the crack initiation happened: 0.4-1.0 mm. The crack initiation probably occurred around a CMOD of **0.8 mm**.

Concerning the crack propagation, the information is obtained by the compliance method: the elastic slope of each reloading period on the bending moment/CMOD curve is compared to the initial one and is related to an increasing crack depth. At the beginning, the calculated crack depth is decreasing, what probably corresponds to blunting and hardening. That’s why we finally take as a reference the maximal compliance we get (corresponding to the third reloading period). We then obtained the following results (Table 14).

According to these results, the crack propagated on a maximal depth of 16.2 mm. We should compare this to the crack propagation we measured on the pipe after the test.

Reloading phase number	3	4	5	6	7	8	9
Normalised elastic slope	1	0.96	0.89	0.58	0.54	0.41	0.42
Estimated crack growth (mm)	0.2	0.6	1.6	8.3	9.6	16.2	15.5

Table 14: Crack propagation results by the compliance method

Mock-up destructive examination

The destructive expertise allows to precisely estimating the total crack propagation that occurred during the test. Results are contained in Table 15. The maximal crack propagation is reached more or less in the centre of the defect (Fig. 60) and reaches 28.2 mm. This is much more than the estimated propagation calculated through the compliance method. But we have to keep in mind that one assumption of the method is that the crack propagates as much on both sides than in the middle of the defect. But average values should be compared: the 16.2 mm estimation is still lower than the measured 21.9 mm, but seems then more reasonable.

Position (mm)	0	10	20	30	40	50	60	70	80
Crack propagation (mm)	0	18.7	22.3	24.7	27	27.3	26.3	25	25.7
Position (mm)	90	100	110	120	130	140	150	160	169
Crack propagation (mm)	25.3	26.5	26.8	24.8	23.8	20.7	18.8	9	0

Table 15: Crack propagation: measurements

It should also be noticed that the defect initiated and then propagated, on a long distance, in a pure ductile mode (Fig. 60). There is no trace of any brittle fracture concerning the propagation of this crack.

We also made different section cuts in this piece (Fig. 61) and could then observe the position of the notch regarding the fusion line as well as the crack path.

Firstly, the notch had been correctly positioned [16] relatively to the fusion line: the distance between the axis of the notch and the fusion line varies between 0.9 and 1.8 mm (the interface being not so straight).

Concerning the crack path, the defect basically followed the fusion line, getting a bit closer to the interface and remaining in the buttering layer. The crack propagation occurred in a transdendritic way, confirming the EBM observations: the propagation occurred in a pure ductile mode.

Figure 60: Crack propagation: fracture profile and EBM picture

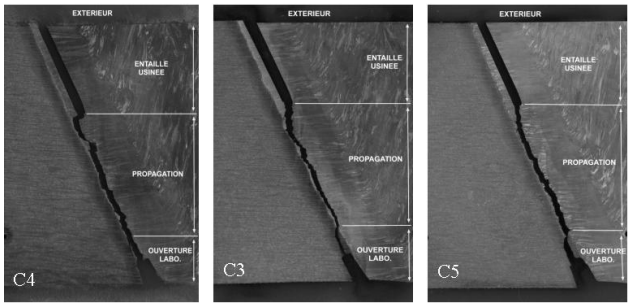

Figure 61: Crack propagation

1.5. Analysis

The objectives were to assess the capabilities of existing analysis techniques for the prediction of the behaviour of a DMW pipe component containing a crack, located parallel to, and at or close to, the fusion line. Three basic methodologies will be examined: conventional flaw assessment methods, more advanced J methods and local approach-based methods. The results of these analyses will be benchmarked against the results of the pipe bend test. Three phases are ongoing:

- test design analyses to assure the fulfilment of the objectives with the test facility capabilities
- pre-test analyses to make a blind test prediction on the bases of pre-test knowledge of some parameters
- post-test analyses to make methods comparison and validation with a good knowledge of each parameter.

Test-design analysis

Different constraints have been fixed to the test:

- 4-point bending test with "constant" bending load between inner span needs to define an off-set value: 285 mm
- crack initiation for a "reasonable" load level
- "sufficient" crack growth to confirm a "ductile" behaviour when the crack reach the fusion line
- maximum load "less" than maximum test facility capability
- maximum displacement "less" than maximum test facility capability
- "constant" 300 °C temperature in the mock-up during the test
- "refined" instrumentation for "detailed" comparison with analysis.

In order to fulfil all these requirements, different parametric studies have been done using "expected" material properties (strength and toughness), real geometry and expected crack location and depth. All these studies, with different offsets, different crack depths and different toughness levels have been done through simplify J estimation schemes (Fig. 62).

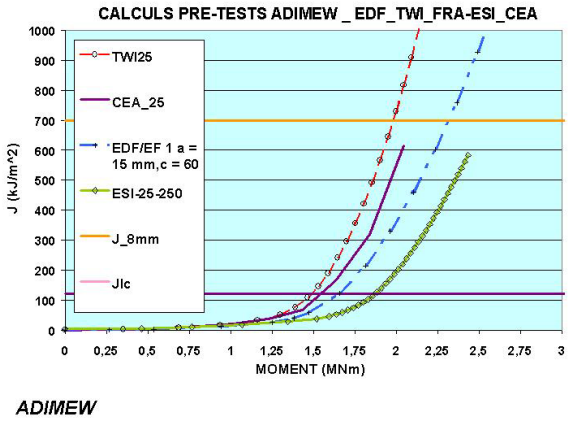

Figure 62: Test-design analyses

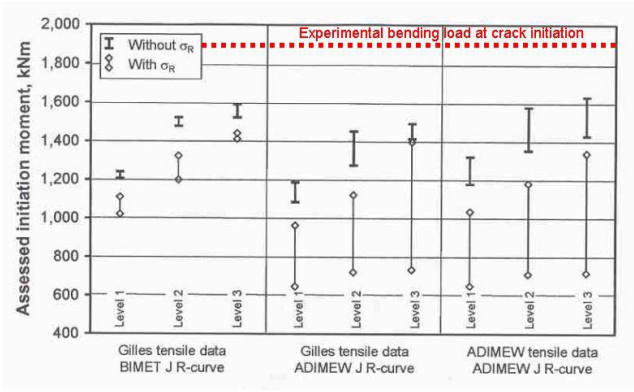

Figure 63: SINTAP method – pre-test analysis

Pre-test analysis

The second level, using some pre-measured material properties, the correct piping geometry and crack depth, with a reasonable precision in the crack location (1.5 mm from the fusion line), has been done by different participants with engineering and finite element method [22, 23, 24, 25].

The results are presented in Table 16 and Fig. 63 for the SINTAP FAD [26] method.

	Participant 1	Participant 2	Participant 3	Participant 4	Participant 5
Method	SINTAP FAD [26]	RSEM Js [27]	Finite element	Finite element	Engineering method
Initiation bending moment (MN.m)	1,425	1,6	1.5	1,55	1,84
Max. bending moment and ductile tearing	1,6 for Δa = 0.5 mm	2.1 for Δa = 9.5 mm	2.1 for Δa = 13 mm	n/a	Max. moment for Δa > 25 mm

Table 16: Pre-test analysis – results comparison

The results are similar except for Participant 5. The experimental initiation bending moment is around 1.9 MN.m and the maximum moment less than 2.1 MN.m with a maximum value of 28 mm ductile crack growth. The crack initiation predictions are very conservative and the maximum load evaluations are reasonable with an underestimation of the ductile crack growth.

Post-test analysis

After the end of the material characterization programme, the collection of test data and result of the destructive examination of the mock-up the pre-test hypothesis have been updated and the different assumptions has been reviewed [24, 25, 28, 29]. The crack depth is close to 16.2 mm (instead of 17 mm) and the crack location between 0.9 and 1.7 mm (instead of 1.5 mm). These data confirm that similar geometry as initial pre-test analysis can be used mainly for the finite element approaches. Two engineering methods (R6 and RSEM) are used and two finite-element analyses are done.

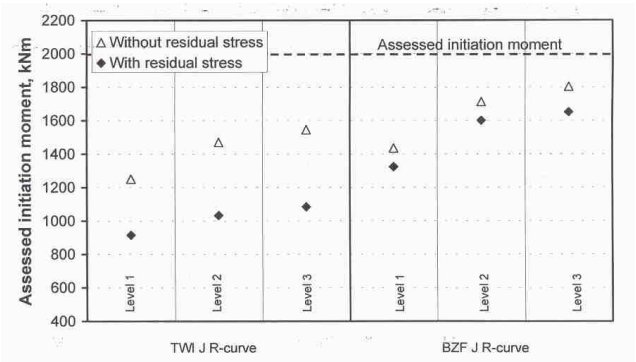

Figure 64: SINTAP method – post-test analysis

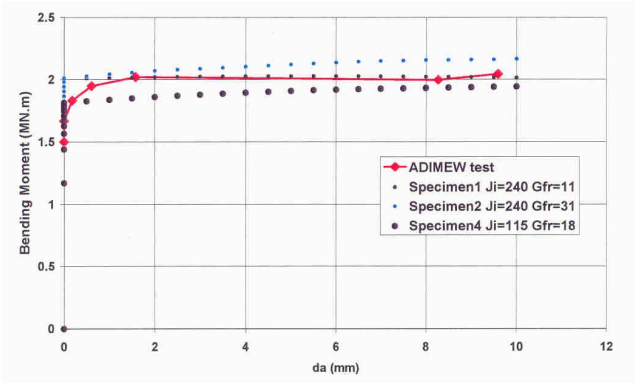

Figure 65: RSEM with CEA improvements – post-test analysis

In parallel to these engineering methods, two finite-element analyses have been performed.

One of them analyses the crack behaviour using a global approach based on the tearing force J. The relevance of this approach for crack initiation prediction has been tested on a bimetallic CT specimen. The refined mesh used is partly presented on Fig. 66. The load versus CMOD prediction is compared to the test records on Fig. 67. The crack initiation prediction is presented on Fig. 68: applied displacement of 95 mm for the simulation versus an experimental value of 115 mm.

The main conclusions of this first study are:

- The force displacement behaviour is poorly reproduced. We consider that this is due to the impossibility of having equal pipe displacements at the two loading points with the test rig used in ADIMEW.
- The differences on forces do not have an important effect on the moment and the crack behaviour, as described by the moment-CMOD curve is very well reproduced.
- The moment value at the crack tip location is the governing load parameter of the crack opening. Therefore, our simulation of the cracked DMW is reliable.
- Residual stresses do not seem to influence the crack initiation as shown by the CMOD evolution. This may be due to stress redistribution induced by yielding. A similar observation has been made on the smaller BIMET component.
- The J value corresponding to the experimentally estimated tearing initiation displacement is much higher than the J initiation value measured on a CT specimen. One cannot conclude that the DMW cracked pipe is more resistant than a bimetallic specimen used as a reference in defect assessments for two reasons. The CT was a cracked specimen, and the defect in

the pipe is a machined notch with a tip radius which may delay crack initiation. Second, detection of initiation during the pipe experiment is inaccurate and a lower value is expected from post-test measurements.

More detailed information on crack opening, estimation of crack extension, determination of the exact crack location, micrographic observations of the crack surfaces would be useful to understand the crack growth behaviour.

Analyses of the crack growth behaviour of the ADIMEW DMW should be conducted using ductile damage models.

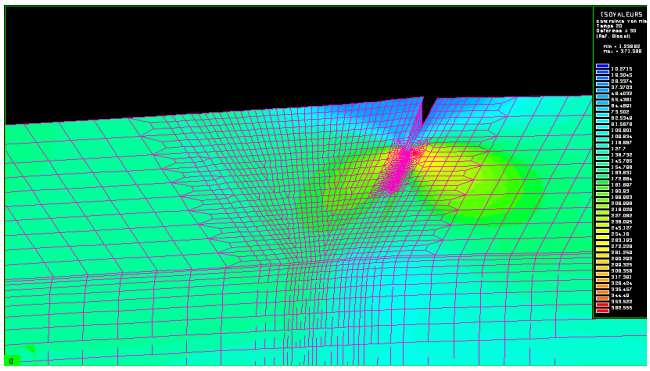

Figure 66: First finite-element model

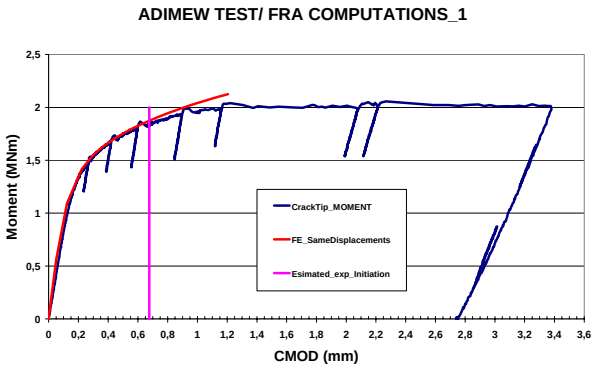

Figure 67: CMOD comparison between FEM and test records (first model)

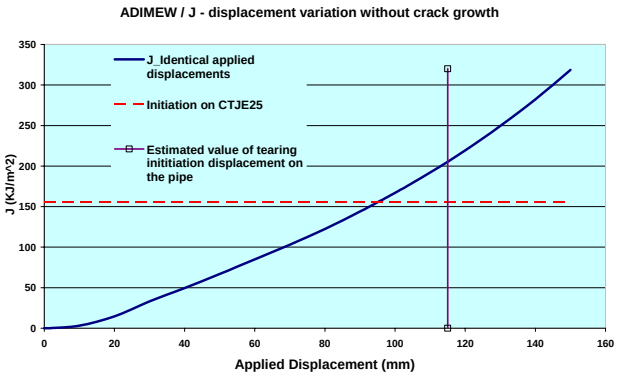

Figure 68: Comparison of crack initiation displacement between FEM prediction and test measurement

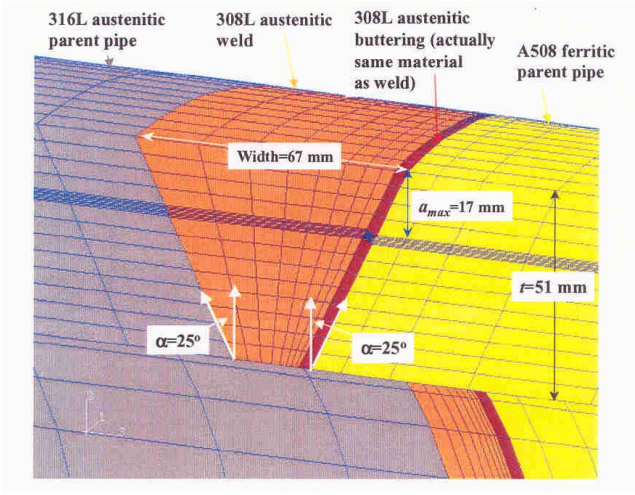

Figure 69: Second finite-element model

A second evaluation has been done through finite element models of the test, with similar approaches, based on J estimation, but without any residual stress consideration).

The mesh refinement is presented on Fig. 69 and 70. The simulation CMOD versus load is compared to test records on Fig. 71. The crack initiation and crack growth are presented on Fig. 72 and 73. The results of the prediction are: a bending moment at crack initiation of 1.95 MN.m for an experimental value between 1.9 and 2 MN.m, and a maximum ductile crack growth of 9 to 12 mm for an experimental value around 25 mm.

The major comments are:

- gross yielding of the pipe assembly occurs in the 316L parent pipe, away from the location of the defect commencing at a plastic yield moment of about 1.6 MN.m. The plastic yield moment is insensitive to crack depth for the range of a_{max} considered. Tearing and stability of

the defect are therefore controlled primarily by the tearing resistance of the buttering material and by its changing size and shape, with little interaction with the applied load

- analysis should tend to over-predict the value of loading parameters (bending moment, RAM displacement) at crack initiation perhaps due to neglect of welding residual stresses in the computation, slightly for crack initiation, but probably no consequences on large ductile tearing
- these numerical predictions are based on uniform crack growth along the crack front and don't consider the rapid reduction of J from the middle of the extremities of the crack
- the use of fracture toughness resistance curve extrapolated way belong the range of valid toughness data measured on small scale tests remains an important open question
- the large extent of tearing observed in the test should not be treated with undue alarm; it's a consequence of the maximum RAM displacement applied.

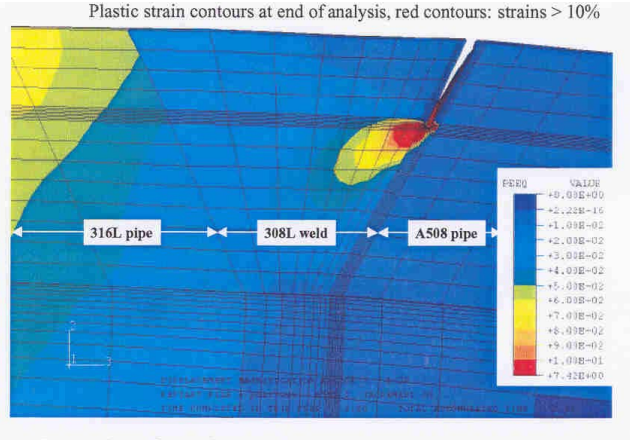

Figure 70: Stress field around the crack front

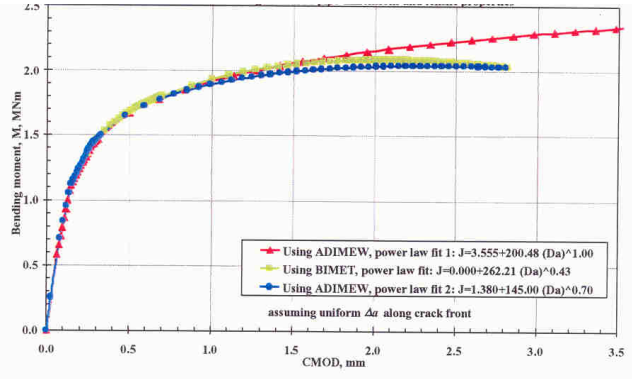

Figure 71: CMOD comparison between FEM and test records (second model)

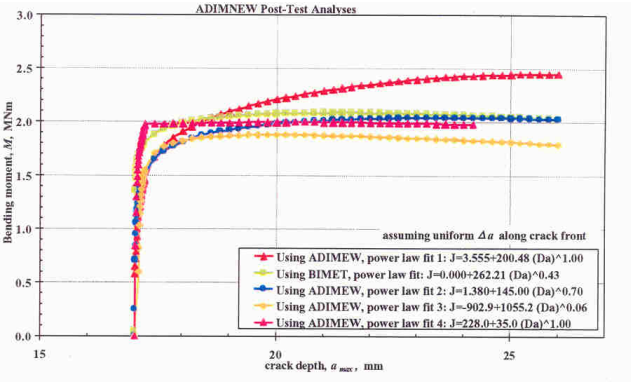

Figure 72: Crack initiation and crack-growth prediction by FEM

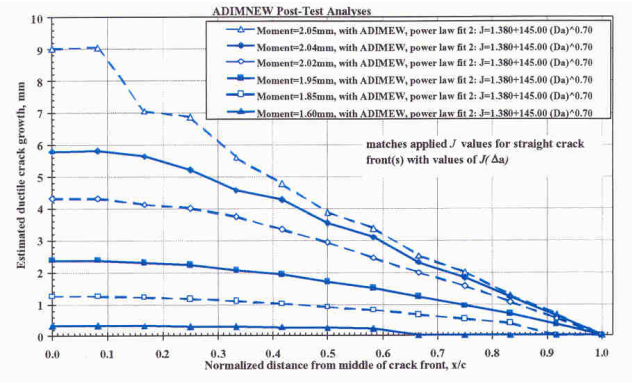

Figure 73: Crack-growth prediction along the crack front

A complementary FEA has been done by CEA [32] to simulate the ductile tearing crack growth.

Complementary analysis on CT specimens

As presented in Section 2.2, toughness material characterisation has been obtained through the CT25 test specimen, a series of tests with pre-cracked specimen close to the standard, and a second series on notched CT specimens, with the same notch type as the AD02 mock-up tested. In order to improve the understanding of the differences, some computation of both type of tests have been done using the finite-element method [30].

The crack tip geometry has significant effect on the stress and strain field close to the crack tip, but the J value curves with different notch radius are close to each other (Fig. 74-75)

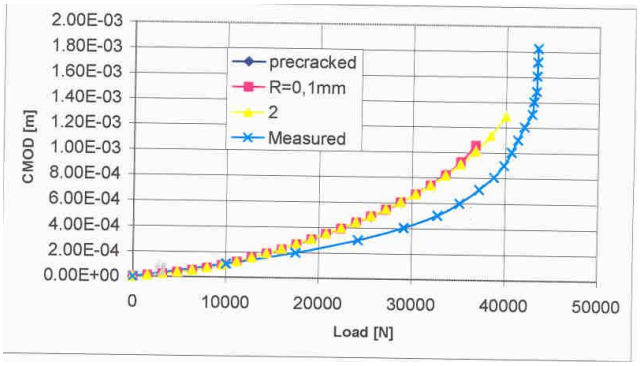

Figure 74: CMOD versus load for pre-cracked and notched CT specimens

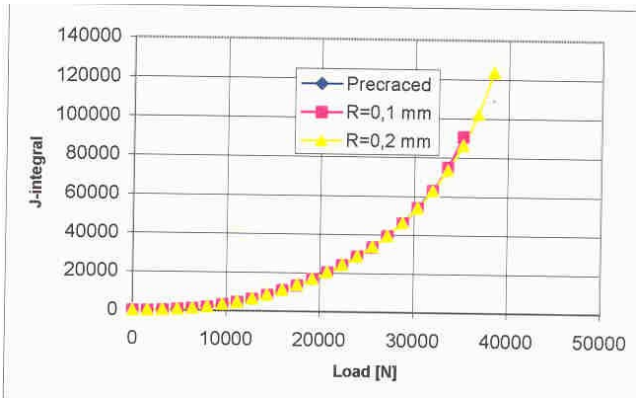

Figure 75: J versus load for pre-cracked and notched CT specimens

Complementary analysis on VVER technology

A specific model of the ADIMEW test has been developed. And after checking the agreement on the ADIMEW test, the same model has been used with specific VVER dissimilar weld materials [31]. The VVER material properties are presented in Table 17.

08KH18N12T austenitic steel						
T = 20 ° C					T = 350 ° C	
R_m (MPa)	$R_{p0.2}$ (MPa)	A_5 %	Z %	KCU 2 J/cm^2	R_m (MPa)	$R_{p0.2}$ (MPa)
509	196	40	55	-	-	167
15H2MFA ferritic steel						
T = 20 ° C					T = 350 ° C	
R_m (MPa)	$R_{p0.2}$ (MPa)	A_5 %	Z %	KCU 2 J/cm^2	R_m (MPa)	$R_{p0.2}$ (MPa)
539-735	431	14	50	78	490	392
EA400/10T weld material						
T = 20 ° C					T = 350 ° C	
R_m (MPa)	$R_{p0.2}$ (MPa)	A_5 %	Z %	KCU 2 J/cm^2	R_m (MPa)	$R_{p0.2}$ (MPa)
539	343	25	30	88	441	245

Table 17: VVER materials properties

Figures 76 and 77 confirm the reasonable agreement between test and simulation. Figures 78 and 79 present comparative results between VVER and ADIMEW technology.

The comparison between the calculated and measured ram-force – ram displacement; ram force – CMOD; moment – CMOD curves can be seen in Fig. 76-77. The curves show good agreement on the ferritic side. The calculated ram force is higher than the measured one on the austenitic side but the difference is acceptable. The difference can be caused by the flexibility of the collars and the unknown change of the material properties of the arms due to the temperature rise toward the muck-up. The tendencies after the fourth to fifth upload are different from the measured one but these can be caused by the crack initiation and propagation.

Comparing the result of the calculation carried out with ADIMEW and VVER materials the effect of the reduction of the yield stresses can be recognised easily in Fig. 78-79. The tendencies of the

curves are similar since the ADIMEW material has been modified using the yield stress values of the VVER materials due to the lack of exact information about the hardening properties of the VVER materials. Because the reduction of the yield stress is almost the same on both sides, the difference between the ADIMEW and VVER curves is also similar.

The ADIMEW methodology can be transferred to VVER technology, but a minimum comparison of material properties and computations have to be made before drawing some quantitative values of critical crack size.

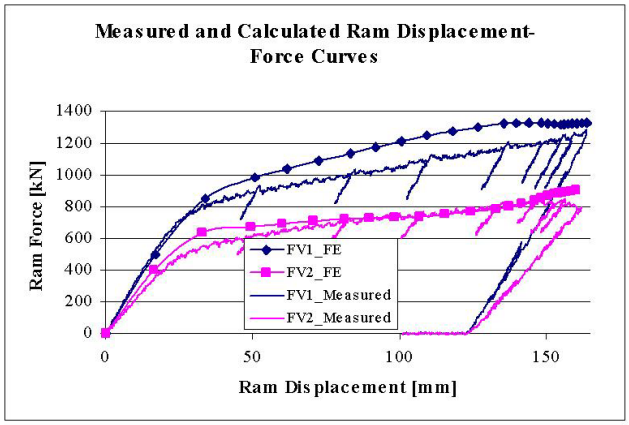

Figure 76: ADIMEW – force displacement curve simulation

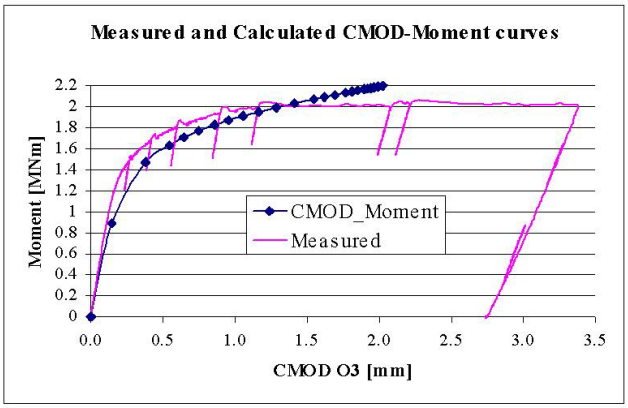

Figure 77: ADIMEW – CMOD bending moment curve simulation

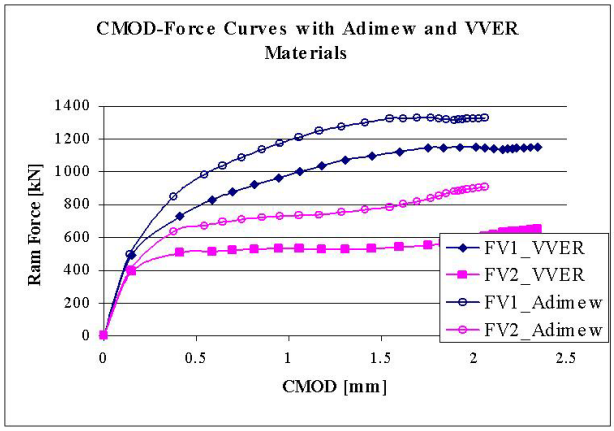

Figure 78: CMOD versus load – comparison of ADIMEW material with VVER material

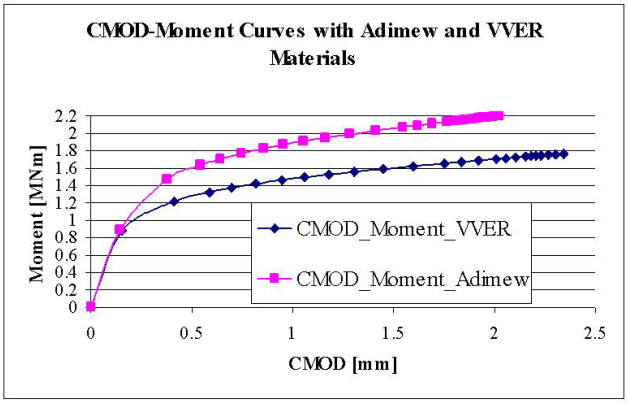

Figure 79: CMOD versus bending moment – comparison of ADIMEW material with VVER material

The ADIMEW prediction methodology can be used for prediction behaviour of VVER technology. Nevertheless, some comparisons on material properties and some computations are needed for quantitative values of critical crack sizes.

Conclusions on the analysis

The major conclusions are:

- Finite-element analysis has successfully modelled the macroscopic deformation and fracture behaviour of the ADIMEW test pipe AD01.
- The analysis could predict the load at initiation of ductile tearing accurately, but the prediction was critically dependent on the degree of representation of the resistance curve derived from

the small-scale fracture test to that of the full-size test pipe in term of crack sharpness, material microstructure, and constraint.

- The analysis successfully predicted the narrow range of load over which significant growth of the defect occurred, a consequence of the low tearing resistance of the buttering material.
- The growth of the defect through the wall but without change in circumferential extent was predicted from the analysis results. It is a behaviour typical of a long-part-through-surface breaking defect in ductile material subject to a uniform tensile stress field.

2. Project evaluation and major conclusions

2.1. Highlights and achievements of the project

The principal focus of the project was the execution of a full-scale test performed on a pipe specimen at 300 °C under four-point bending. The ADIMEW specimen was a nominal 450-mm diameter piping assembly, which contained a ferritic to stainless-steel (A508-308L/309L-316L) dissimilar metal weld (DMW). The DMW was notched at the ferritic/buttering layer interface, to simulate PWR plant experience of cracking in components containing such welds.

The aims of the project were threefold:

(1) quantify the accuracy and conservatism of structural integrity procedures used by the nuclear industry in Europe to predict the behaviour and assess the safety of circumferential defects at the surface of dissimilar metal welds

(2) perform a unique verification of the load-carrying capacity of an industrially representative cracked DMW under operating conditions in a large-scale structural test. To do this, a special assembly was prepared, with circumferential cracks introduced into the surface of a dissimilar metal weld between low-alloy steel and austenitic steel pipes with a diameter of 450 mm

(3) disseminate the results for the benefit of operators, regulators, and research organisations in Europe, in collaboration with the Network for Evaluating Structural Components (NESC), and contribute to the development and verification of analytical methods used to describe the behaviour of an external circumferential surface defect in a DMW.

Consistent with these aims, the experimental objective was to obtain initiation and stable ductile tearing of the defect, confined to take place within the 309L + 308L stainless-steel buttering layer. The analytical challenges arises from the complexity of the structural features, which include a marked variation in material properties across the weld zone, mixed-mode loading and the presence of a weld residual stress field. These are circumstances were the application of classical fracture mechanics concepts is potentially problematic.

2.2. Conclusions

ADIMEW has proven to be a very successful project in which all major experimental and analytical objectives were met. The well-documented fabrication and test reports for ADIMEW, together with the comprehensive materials characterisation data, will be of enduring value in the longer term for future international collaboration directed towards understanding and predicting the structural integrity of complex welded joints. Associated benefits have accrued from the NDE inspection programme during DMW fabrication and the high-quality work undertaken to characterise the 3D distributions of residual stress.

A unique verification of the load-carrying capacity of an industrially representative cracked DMW under operating-condition temperature in a large-scale structural test has been successfully achieved.

The analytical work has succeeded in quantifying the accuracy and conservatism of structural integrity procedures used by the nuclear industry in Europe to predict the behaviour and assess the safety of circumferential defects at the surface of dissimilar metal welds.

The project has demonstrated clearly the synergy that is possible between finite-element analyses and simplified (engineering assessment) methods, and pointed towards the value of using EAMs in conjunction with basic FEAs. Lastly, comparisons between predictions and experimental results have provided important evidence for the validation of EAMs in the assessment of defects in complex welded joints.

The results can be partly applicable, with corresponding precautions, to other DMW designs as VVER technology or Ni-alloy DMW.

The results are being disseminated through conference and journal papers for the benefit of operators, regulators, and research organisations in Europe, in collaboration with the Network for Evaluating Structural Components (NESC). They contribute to the development and verification of analytical methods used to describe the behaviour of an external circumferential surface defect in a DMW.

2.3. Recommendations

Recommendations for best practice

There is a need to 'capture' the experience gained in the ADIMEW project in order to advance best practice in structural integrity assessments of complex welded joints. It is considered that the best way forward in this regard is to formulate a summary of best practice as a consensus view of the technical community following presentation and discussion of the main results of ADIMEW at special sessions at international conferences and meetings, e.g. the ASME Pressure Vessels and Piping Conference or the International Conference on Structural Mechanic in Reactor Technology. It would be equally important to arrive at a consensus regarding the general applicability of the ADIMEW material properties and fracture toughness data, and the extent to which the various analytical methods have been validated by reference to the ADIMEW test. Any views on validation should acknowledge that the current analytical work involved a number of conservative (though not unduly so) blind predictions. Also, it would be necessary to identify clearly any limitations remaining in the developed fracture methodologies (see below). Recommendations of best practice arrived at in this way could then be incorporated as incremental improvements in existing defect assessment procedures (e.g. R6, A16 or RSEM).

Recommendations for future work

(1) The simulation of welding residual stresses by FEA highlighted the range of data that may be obtained using different assumptions. It is important that the experience captured within ADIMEW is assessed to provide "best practice" guidance for the calculation of residual stress profiles in DMWs. To this end, the ADIMEW fabrication report, neutron diffraction data and the post-test materials-property data handbook provide a valuable resource for future studies. These residual stresses don't affect significantly the critical crack size margins, but are important contributors for different other degradation mechanisms and for ageing management of plants.

(2) For nuclear class-1 components, best-practice methods of defect assessment are generally based on considerations of failure avoidance with reference to crack initiation. Further work is needed to improve confidence in predicting the extent and stability of crack growth in DMWs.

(3) More work is needed to develop robust experimental methods to accurately measure fracture toughness properties of heterogeneous regions within DMWs. In particular, miniature specimen tests require further development and validation and plastic eta factors need to be developed for a range of weld mismatch situations. The comparison between notched and pre-cracked specimen has to be confirmed and quantified. Mixed-mode toughness criteria have to be checked.

(4) Consideration should be given to improve experimental methods for 'narrowing' the assessed initiation-moment range in future DMW tests. The use of diverse measurement methods should be considered.

(5) Work is needed to develop further so-called hybrid methods of analysis (EAM supported by FEA), in order to optimise the balance between accuracy of prediction, and that of analytical simplicity versus computational complexity. K estimation scheme and limit-load formulae have to be strongly improved in different existing EAMs.

(6) The local-approach method should be assessed in greater detail as an important contributor tool, and existing “best-practice” guidance should be updated in the light of the promising results obtained within ADIMEW.

(7) The transferability of these results to any other DMW technology has to be confirmed.

3. Conclusions

A large-scale test (16”) at operating conditions (300 °C) of a very safety-significant structure has been conducted successfully on 13 July 2003, with a set of complementary studies performed on residual stresses, material properties, mixed-mode rupture, notch/pre-cracked CT tests, etc.

All the pre- and post-test analyses have been done and the predictions are in reasonable agreement with the test results.

A lot of innovative work has been done:

- residual stress measurement through the wall thickness by neutron diffraction
- material-property evaluation around the fusion line at 300 °C
- analyses through the finite element using J estimation and local approach
- mixed-mode effect analysis.

All these results are compared with more industrial approaches like:

- hole drilling technique for residual stress evaluation on the surface
- notch versus pre-cracked specimen for toughness evaluation
- finite-element versus engineering estimation scheme (mode I, elliptical crack).

Transferability of approaches to other technology, as VVER technology, has been successfully studied.

The DMWs are needed to connect ferritic components with austenitic piping and are used in safety class-1 systems of major LWR plants (PWR, BWR, and VVER). Their integrity without and with hypothetical cracks has to be justified in all conditions of plant life. Due to the complexity of the DMW for fabrication, inspection and analysis, specific projects such as ADIMEW have to be developed to confirm the quality of the present DMW design rules and their behaviour with ageing (cracked). The ADIMEW project is unique in the world and an important step in considering tests and analysis of DMWs, at room and operational temperatures. It can support the validation of different engineering methods, as R6 in the UK [5] or RSE-M [6] in France. A lot of innovative actions developed during this project can be used by different industries (nuclear and non-nuclear), like material-property measurements and residual-stress evaluation.

The success of this project is attributed to:

- mutual interest from industry and research laboratories
- constant progress from BIMET to ADIMEW, with EC support
- practical consequences on safety-class nuclear components
- ten years of common work between 7 of the 8 participants with a successful integration of the Hungarian participants (as number 8)
- the creation of a powerful group of European experts in different fields
- good connection with the NESC network
- results transferable to other designs, e.g. VVER and to non-nuclear pressure equipment
- that all the data are ready to use the ADIMEW test as a major benchmark for structural-integrity analysis of aged (cracked) dissimilar metal welds.

4. References

[1] BIMET, "Structural Integrity of Bi-Metallic Components – Final Summary Report" – Contract FI4S-CT96-0030.

[2] M. F. Cipierre, "Manufacture of two mock-ups with bi-metallic weld of austenitic stainless steel, representing a pressuriser surge nozzle", FRAMATOME-ANP, NFEMT.02.0341, 12 September 2003.

[3] F. Hukelmann, M. Wallendorf, J. Pozuelo Moreno, I. Iacono, "Insertion of a straight defect into the ADIMEW component AD02 by means of Electro-Discharge Machining". JRC-IE report, NSU/FH/2002/10/01, October 2002

[4] J. Margalida, "Arm assembly fabrication report", NORDON report, June 19, 2002

[5] H. Keinänen, A. Laukkanen, P. Nevasmaa, "Fracture and Tensile Testing of the AD01 Mock-Up",. Research report TUO72-033337. VTT Industrial Systems, 26 p., December 19, 2003.

[6] M. F. Cipiere, "Fracture Toughness testing of the 308/309L Buttering: Impact notch toughness- Ductile tearing resistance", FRAMATOME-ANP, NFPMT03.282, November 12, 2003.

[7] JB. Wintle, B. Hayes, M.R. Goldthorpe: "ADIMEW Project: Fracture Toughness Testing of AD01 Dissimilar Metal Weld", TWI REPORT NO: 13219/2/03, November 2003.

[8] G.B. Lenkey, "Report on the effect of defect tip radius on the basis of experiments", Bay Zoltán Foundation for Applied Research, Hungary, October 2003.

[9] A. Laukkanen, H. Keinänen, P. Nevasmaa, "Mixed-Mode Small-Specimen Fracture Tests of the AD01", Component. Research Report TUO72-033350. VTT Industrial Systems, 23 p., December 19, 2003.

[10] C. Ohms, P. Hornak, R. Winpory, "Residual stress measurements by neutron diffraction", JRC-IE report, AGE-ADIMEW (03)-P0025, November 20, 2003.

[11] J.B. Wintle, R. Sanderson, S. Green, "Residual stress measurements by hole drilling of AD01 dissimilar metal weld", TWI report 13219/3/03, November 2003.

[12] Ph. Gilles, "Residual stress analysis report", FRAMATOME-ANP report NFPMR-DC-93 Rev. A, November 20, 2003.

[13] RCC-M Code, 2000 edition, "Design and Construction Rules for Mechanical Components of PWR Nuclear Islands", Paris, AFCEN, Paris

[14] G. Martin, "Spécifications de l'essai ADIMEW – Essai de flexion 4 points sur une liaison bimétallique à l'échelle 1", ADIMEW(02)-P004, May 2002.

[15] Ph. Gilles., "Defect sizing and positioning – Further results", ADIMEW(02)-P006, July 2002.

[16] F. Hukelmann, M. Wallendorf, J. Pozuelo Moreno, I. Iacono, "Insertion of a straight defect into the ADIMEW component AD02 by means of Electro-Discharge Machining". JRC-IE report, NSU/FH/2002/10/01, October 2002

[17] G. Martin, J.M. Cerdan, "Plan d'instrumentation de la maquette ADIMEW", ADIMEW(02)-P010, October 2002.

[18] G. Martin, "ADIMEW European Project: Test Procedure", ADIMEW(03)-P001, April 2003.

[19] Ph. Gilles, "Calculs de l'essai ADIMEW", ADIMEW(03)-P016, September 2003

[20] G. Martin, "ADIMEW European Project: Test Quick Look Report, ADIMEW(03)-P018, August 2003.

[21] G. Martin, A. Menard, "European Project ADIMEW: Overall Test Report", EDF report ADIMEW(03)-P024, December 2003.

[22] A. H. Sherry, S. K. Bate, D. W. Beardsmore, "Pre-test assessment of the ADIMEW dissimilar metal weld", SERCO SA/EIG/12428/R001, February 2003.

[23] Y. Kayser, "Pre-test analysis of ADIMEW project", CEA report SEMT/LISN/RT/02-035/A, November 26, 2002.

[24] Ph. Gilles, "Report on Post-test Finite Element Analysis", FRAMATOME-ANP report NFPM-DC-5 Rev. A, November 20, 2003.

[25] JB. Wintle, B. Hayes, M.R. Goldthorpe: "Finite Element and Fracture Mechanic Analysis of the Dissimilar Metal Weld Test", TWI report 13219/4/03, November 2003

[26] SINTAP : "Structural Integrity Procedures for European Industry", November 1999

[27] RSE-M Code, "Rules for In-service Inspection of Nuclear Power Plant Components", 1997 edition + 1998 and 2000 addenda, AFCEN, Paris

[28] A. H. Sherry, D. W. Beardsmore, "Post-test assessment of the ADIMEW dissimilar metal weld", SERCO SA/EIG/12428/R002, December 2003.

[29] Y. Kayser, S. Chapuliot, "Post-test analysis of the ADIMEW project by analytical methodologies", CEA report SEMT/LISN/RT/03-041/A, November 21, 2003.

[30] S. Szavai, G. B. Lenkey, "FE and sensitivity analysis of CT specimen", Bay Zoltán Foundation for Applied Research, Hungary, May 2003.

[31] S. Szavai, "Report on FE post-test and sensitivity analyses", Bay Zoltán Foundation for Applied Research, Hungary, October 2003.

[32] S. Marie, S. Chapuliot, "Complement of the interpretation of the ADIMEW test on a cracked pipe containing a bimetallic weld", CEA report SEMT/LISN/RT/04-016/A, 1 June 2004.